A THESIS SUBMITTED TO
THE GRADUATE SCHOOL OF NATURAL AND APPLIED SCIENCES
OF ÇANKIRI KARATEKİN UNIVERSITY

ENHANCEMENT THE DAMS CONCRETE PERFORMANCE USING RECYCLED HDPE PLASTIC ADDITIVES

IN PARTIAL FULFILLMENT OF THE REQUIREMENTS
FOR
THE DEGREE OF MASTER OF SCIENCE
IN
CIVIL ENGINEERING

BY

WALAA WAQAR ALI ALI

ÇANKIRI

2023

ENHANCEMENT THE DAMS CONCRETE PERFORMANCE USING RECYCLED HDPE PLASTIC ADDITIVES

By Walaa Waqar Ali ALI

February 2023

We certify that we have read this thesis and that in our opinion it is fully adequate, in scope and in quality, as a thesis for the degree of Master of Science

Advisor **:** Assoc. Prof. Dr. Cihan DOĞRUÖZ

Examining Committee Members:

Chairman **:** Assoc. Prof. Dr. Cihan DOĞRUÖZ
Civil Engineering
Çankırı Karatekin University

Member **:** Asst. Prof. Dr. Başak VARLİ BİNGÖL
Civil Engineering
YıldızTechnical University

Member **:** Assoc. Prof. Dr. Murat YAYLACI
Civil Engineering
Recep Tayyip Erdoğan University

Approved forthe Graduate School of Natural and Applied Sciences

Prof. Dr. İbrahimÇİFTÇİ
Director of Graduate School

I hereby declare that all information in this document has been obtained and presented in accordance with academic rules and ethical conduct. I also declare that, as required by these rules and conduct, I have fully cited and referenced all material and results that are not original to this work.

Walaa Waqar Ali ALI

ABSTRACT

ENHANCEMENT THE DAMS CONCRETE PERFORMANCE USING RECYCLED HDPE PLASTIC ADDITIVES

Walaa Waqar Ali ALI

Master of Science in Civil Engineering

Advisor: Assoc. Prof. Dr. Cihan DOĞRUÖZ

February 2023

Enhancing concrete dam structure is a main target to improve dams performance against various stresses reflection and deformation. Utilizing HDPE (high-density polyethylene) protects and improves reinforced dam concrete strength and reduce the weight of total concrete with enhances the foundation performance and cost. The experimental work was carriedout using a model of concrete dam to study response and resistance against subjected overflow effect. The laboratory experimental program marked as two groups; the simulation tests specify Koyna Dam as a sample for validation, and extend the study to investigate three different types of dams with different sizes. The recent research results indicate that the HDPE with a percentage of 5%, size (5*20) mm and fc 25 has a significant improvement on the behavior of concrete under the same conditions, also in general the shear strength improved with respect to HDPE and the results observed more concrete ability with it. Finally, HDPE presents a superior results interms of concrete mechanical characteristic in all dams crest heights.

2023, 71 pages

Keywords: HDPE, Shear strength, Conventional concrete, Crest

ÖZET

GERİ DÖNÜŞTÜRÜLMÜŞ HDPE PLASTİK KATKI MADDELERİ KULLANARAK BARAJLARIN BETON PERFORMANSININ ARTTIRILMASI

Walaa Waqar Ali ALI
İnşaat Mühendisliği, Yüksek Lisans
Tez Danışmanı: Doç. Dr. Cihan DOĞRUÖZ
Şubat 2023

Beton baraj yapısının iyileştirilmesi, farklı gerilmelerin yansıması ve deformasyonu oluşturan barajların performansını iyileştirmek için kullanılan ana hedeftir. HDPE'nin etkisi, betonarme baraj betonunun mukavemetini korur ve geliştirir ve temel performansını ve maliyetini artıran toplam betonun ağırlığını azaltır. Bu çalışmada, maruz kalınan taşma etkisine karşı tepki ve direnci incelemek için bir beton baraj modeli kullanılarak deneysel çalışma yapılmıştır. Laboratuvar deney programı iki grup olarak işaretlenmiştir. Simülasyon testleri, doğrulama için bir örnek olarak Koyna Barajı'nı belirlemekte ve çalışmayı farklı boyutlarda dört farklı tipte barajı araştırmak üzere genişletmektedir. Son araştırma sonuçları, %5'lik bir yüzdeye, boyuta (5*20) mm ve fc25'e sahip HDPE'nin aynı koşullar altında betonun davranışında önemli bir iyileşmeye sahip olduğunu, ayrıca genel olarak HDPE'ye göre kesme mukavemetinin arttığını ve Sonuçlar onunla daha somut bir yetenek gözlemledi. Son olarak, HDPE, tüm baraj kret yüksekliklerinde üstün bir beton mekanik özelliği sonuçları sunar.

2023, 71 sayfa

Anahtar Kelimeler: HDPE, Kesme dayanımı, Konvansiyonel beton, Kret

PREFACE AND ACKNOWLEDGEMENTS

I would like to thank my father Waqar BDEN, Mother Eman SAEED, husband Mustafa AL-AZAWY, brothers Dr. Wael, Yasir and Asser, sister Hala, and my thesis advisor, Assoc. Prof. Dr. Cihan DOĞRUÖZ for his patience, guidance and understanding.

Walaa Waqar Ali ALI
Çankırı-2023

CONTENTS

LIST OF SYMBOLS

cm	Centimeter
m	Meter
mm	Millimeter
MPa	Megapascal
sec	Second
%	Percentage

LIST OF ABBREVIATIONS

CAD	Computer aided design
CFR	Concrete forced rockfill
CFRD	Concrete face rockfill dam
CFRP	Carbon fiber reinforced polymer
DOF	Degrees of freedom
FC	Facter of safty
FE	Finite element
FEM	Finite element method
FRC	Fiber reinforced concrete
FRP	Fiber rienforced plastic
HDPE	High density polyethylene
HFRC	Hybridfiber reinforced concrete
IDA	Incremental dynamic analysis
LHS	Latin hypercube sampling
MCE	Maximam credible earthquake
MDE	Maximam design earthquake
PA	Pdymides
PAN	Acrylics
PE	Polyehylene
PES	Polyester
PET	Poly ethylene terephthalate
PF	Polypropylene fiber
PFRC	Polypropylene fiber reinforced concrete
PGA	Peak ground acceleration
PP	Polypropylene
PSO	Particle swarm optimization
PVA	Polyvinyl acetate
RC	Reinforced concerete
RCC	Roller compacted concrete
SVM	Support vector machine

LIST OF FIGURES

LIST OF TABLES

1. INTRODUCTION

1.1 Overview

Concrete dams are buildings which used to store significant amounts of water for a variety purposes. The presence of tensile stress is not permitted in the design approaches for gravity concrete dams. It should be evaluated depending on the compressive stress happening in the dam body. In addition, the stipulated concrete strength for a concrete arch dam should be established taking into account the permissibility of tensile stress in the dam body and the dam body in a multiple-axis stress condition (Campos *et al.* 2016). To avoid cracks in the dam concrete body, the identified concrete strength of the dam body for the concrete arch dam without lateral carrying should be determined by reduplicate the first principal stress (maximum compressive stress) occurring at a given point in the dam body by a safety factor of four or greater (Deoda *et al.* 2020). As a result, concrete gravity dams built in accordance with the current specification are likely to fracture amid severe shaking, such as maximum credible earthquakes. To maintain dam serviceability, dangerous cracking in the dam body should be avoided in advance. In hydraulic concrete constructions, cracks are the most common indication of age and illness. They could make dam bodies more stressed (De Falco *et al.* 2017). Due to the deprivation of integrality and impermeability of concrete, cracks have a significant impact on the bearing capacity and stability of concrete structures. This might eventually result in collapse, modifications in regular operations, or a loss in the dam's engineering advantages. Cracks impact a huge number of concrete dams, including the arch dam Koelnbrein in Austria, in Russia the SayanoShushenkaya gravity-arch dam, and the Shimen arch dam in China (Wu *et al.* 2016). As a result, with the building of a significant number of concrete dams, it is critical to investigate the evolution rules and develop the concrete dams crack safety monitoring models.

1.2 Fiber Reinforced Concrete

The fiber rainforced concrete materials have increasing structural integrity. As a composite material, fiber reinforced concrete comprises midum discrete fibers that are randomly orientated and evenly dispersed (Ismail and Al-Hashmi 2008). Fiber Reinforced Concrete (FRC) is based on more than 50 years of expertise using steel fibers that are randomly distributed in a concrete matrix. Other fiber kinds have recently been found to be suitable for structural concrete components and to function similarly (Löfgren 2005). Concrete with dispersed fibers is used to make fiber reinforced concrete. When fibers are mixed with concrete, the strength and crack pattern are improved. Several little fractures appear in fiber reinforced concrete fault behavior rather than one or two bigger fissures in typical concrete. Fibers may be made out of a variety of materials. The fiber types are divided into four rescores by the ACI 544 (Yimer and Aure 2020). They were utilized to enhance the characteristics of concrete and cement composites. polyester (PES), polypropylene (PP), HDPE are among the synthetic fibers used to include cement matrices (Meran *et al.* 2008). Figure 1.1 shows several instances of different commercially available fibers. Fiber's geometrical and mechanical qualities change according on their impacts, giving concrete its own set of characteristics. Some fiber kinds are utilized to increase toughness and decrease crack widths, while others are used to reduce shrinkage cracking (Aire *et al.* 2011). There are many materials can be used in this field, one of them is the Polypropylene Fiber Reinforced Concrete (PFRC). Concrete structure can be improved by adding the fibrous materials (Xu *et al.* 2018). Plastic shrinkage concrete is a constant source of concern in the concrete industry (Hasan *et al.* 2011). Concrete cracking may expose it to harmful factors, which leads to corrosion of the steel inside, due to the drying shrinkage factor. By controlling the drying shrinkage in concrete, cracking will be minimized and therefore improve the durability of structure with a lengthy life span. The plastic shrinkage cracking stage was the focus of the experimental data on the performance of polypropylene fibers (PF) reinforced concrete. It improves the brittleness of concrete and its poor resistance to shear and tensile pressures.

Vibrations, wind, earthquakes, and other forces are difficult to withstand in plain concrete. Adding fibers to concrete improves its resistance to failures. As shown in Figure 1.2, the theoretical models use an appropriate by applying PFRC (Xu *et al.* 2018).

Figure 1.1 Some of the commercially existing fibers

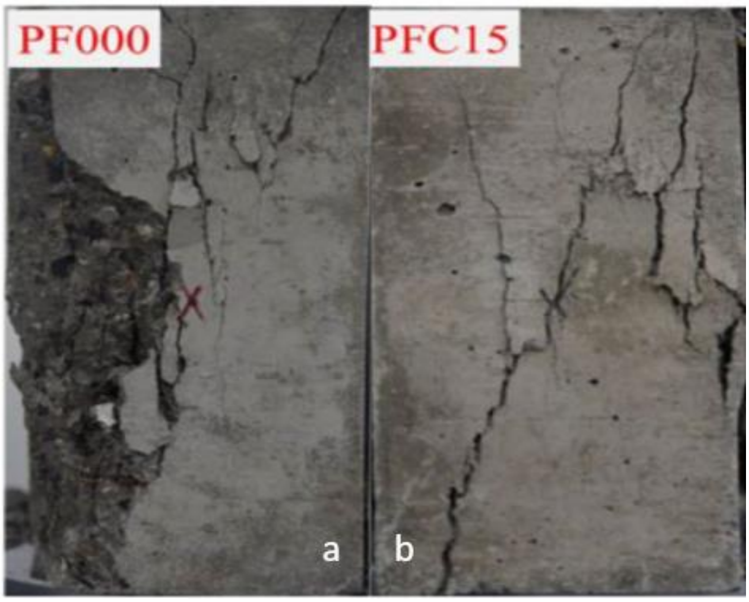

Figure 1.2 Comparison between the strength of concrete without PFRC **(a)** and with PFRC **(b)** (Xu *et al.* 2018)

1.3 Problem Statement

Concrete gravity dams are prone to fracture under lateral stresses because they cannot withstand high tensile stress. Once cracking begins, it will spread throughout the dam body. Although dam body fractures may not necessarily indicate dam failure, they do reflect faults that affect structural resistance and may lead to dam body failure. As a result, concrete cracking is a significant aspect in determining the safety of gravity dams, and any cracking in the dam body should be controlled in advance to assure dam safety. To avoid this, the major goal of improving the dam's concrete construction is to boost concrete characteristics. Many strategies for increasing ductility and resisting shear force have been proposed. Shear reinforcements and steel studs are commonly utilized these days, but fiber demonstrates a significant improvement.

1.4 Objective of Study

This research going to determine how the incorporation of HDPE into the concrete of the dam affects the material's tensile strength after it has been used. Shear behavior of concrete under HDPE polymer-fiber circumstances compared to shear behavior of concrete under normal conditions; studying the performance of HDPE polymer-fiber in various dam environments. To achieve this goal, concrete samples will be subjected to a variety of fibers and analyzed using the following methods: shear behavior of concrete under HDPE polymer-fiber circumstances versus shear behavior of concrete under normal conditions.

1.5 Thesis Outline

There are five chapters in this thesis. The first chapter covers basic concrete specifications, problem formulation, and the types of polymer additives that can improve concrete durability.

The second chapter gives an overview of the impacts of plastic fibers on concrete behavior in various experiments gathered from various investigations.

In chapter three, the experimental program is described, which includes the examined parameters, work methods, and testing of HDPE added to concrete specimens.

The work's outcome and calculation are discussed in Chapter 4.

Finally chapter 5 presents conclusions and recommendations along with the envisioned future Works.

2. LITERATURE REVIEW

2.1 Introduction

Due to the enormous cost of constructing large dams, therefore emerged roller compacted concrete (RCC) and concrete-faced rockfill (CFR) as alternatives to traditional dams. As for their seismic properties, dams (RCC), (CFR) are still unknown so far. The greatest danger is when horizontal cracks occur dams have they raise additional issues; The horizontal cracks provide the greatest risk; If a horizontal crack arises inclined towards the upstream face of an arch gravity dam during continuous earthquake shaking (ACI Committee 2014), a detached concrete block may fall progressively into the reservoir. The emergence of fractures in a monolithic, isotropic dam is hard to predict. Crack geometry and the approximate positioning of discrete cracks may be discussed in fracture mechanics. Fractures and joint openings may not pose a threat to the dam's seismic stability.

Lower Crystal Springs gravity dam the 57 m high (Jaiswal and Jain 2004), that is located near to the San Andreas Fault, was found undamaged by the 1906 San Francisco earthquake, as seen in Figure 2.1. The dam was made of a huge number of interlocking concrete pieces (Getachew 2018, Pelecanos 2013).

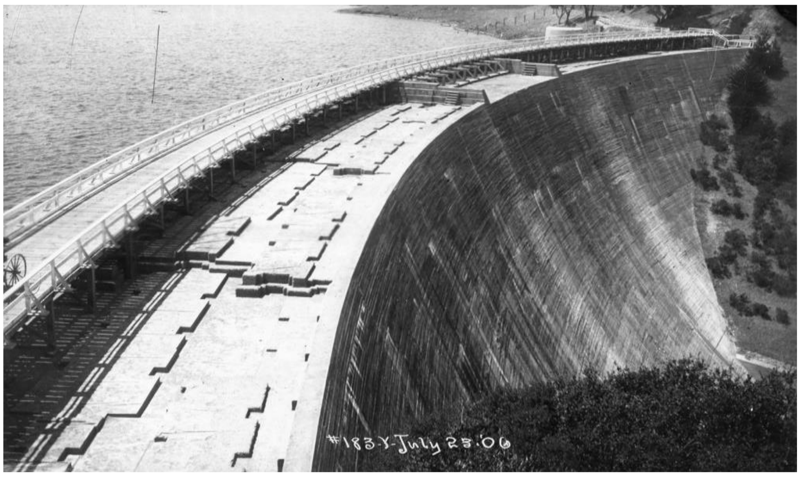

Figure 2.1 Lower Crystal Springs gravity dam no damage occurred after having been shaken by the 1906 San Francisco earthquake (Jaiswal and Jain 2004)

Since the introduction of the face rockfill dam, seepage has been a major concern in the engineering of dams. Leakage and uneven seepage will occur due to design defects in the dam's body and anti-seepage, as well as face damage caused by compression and fractures, and other issues. When the face sustains serious damage, the role it ordinarily performs to prevent seepage is disrupted. As a result, seepage discharge increases and passes through the bedding and transition zones, resulting in cracks and the eventual collapse of the face. A high seepage discharge might even lead to dam collapse. In China tragic accidents have been happened during the setting up of concrete slab rockfill dams in abroad (CFRD). When the operation of the San Banxi Dam is going on, regional damage at the down part of the face construction joint causes external stress, causing the vertical joint to partially collapse, resulting in significant leakage through the dam body of up to 30 L/s (Liang *et al.* 2020). Figure 2.2 depicts how the dam's operation and the safety of a continuous seepage were changed significantly.

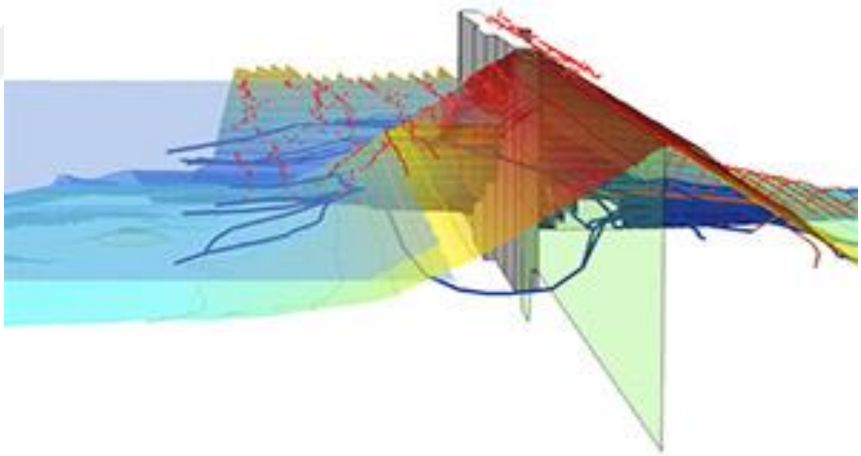

Figure 2.2 Dam seepage due to cracks.

The progression of technology improves the standard of living for humans but comes at the expense of the natural environment. Trash is produced as a byproduct of all three of the following: manufacturing, industrial services, and municipal solid wastes (Silva *et al.* 2020, Godfrey2019).

The fast rise in awareness of the need to protect the environment has made the problems with rubbish disposal much worse. Management of solid waste is recognized as one of the most significant environmental concerns facing the globe today. Since there is a shortage of space in landfills and costs continue to grow, using rubbish as a resource has emerged as a competitive option for waste disposal. Plastic bottles that have been thrown away are the primary contributor to the problem of solid waste disposal. PET, PETE, and polyester are all types of polyethylene terephthalate (PET), which is a material that is frequently seen in containers for beverages and water (bottles). This is detrimental to the health of the ecosystem since used plastic bottles are difficult to decompose and need processes that are laborious and time consuming to recycle and reuse. The construction industry is looking more and more for materials that are both cost-effective and trustworthy in order to increase the strength of concrete (Shi *et al.* 2019, Nikbin *et al.* 2016).

2.2 Experimental and Analytical Researches

2.2.1 Dams

The seismic performance of dams RCC and CFR, where a qualitative assessment of the seismic impact was made, illustrated in the Figure 2.3 deformation of concrete slab derived from dynamic analysis, and different challenges and weaknesses were analyzed (Wieland and Fan 2004).

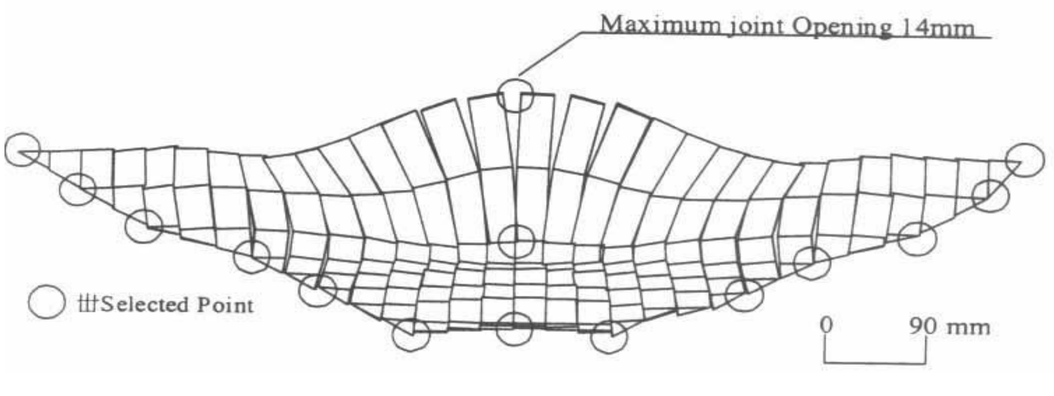

Figure 2.3 Concrete slab deformation of obtained from dynamic analysis

They discovered that RCC and CFR dams are more cost-effective than conventional dams. Because no seismic safety measures exist for these dams, their seismic performance must be extensively evaluated using all available data.

Also produces very large pressures on the dam's body, due to the cross-canyon earthquake component; this can be seen in Figure 2.4.

Figure 2.4 SefidRud buttress dam cracks at the crest of the 106 m high (Jaiswal and Jain 2004)

As may be seen in the images located above: A local compression failure of the deck slab occurred at the intersection of two adjoining monoliths on the left, and cracks formed in the concrete slab of distinct blocks on the right as the dam approached its axis. On June 21, 1990, the Manjil earthquake occurred in the Alborz mountain range in the northwest of Iran. This earthquake triggered breaches near the 106-meter-high SefidRud buttress dam (Berton *et al.* 2009).

Cracks will form along the horizontal construction interfaces in the highly stressed central upper part of the dam as a result of the qualitative evaluation that was performed on the RCC dam. Despite this, the seismic safety of the dam under ground vibration was found to be good. This is due to the fact that cracks will form in the highly stressed central upper part of the dam. During periods of intense ground shaking, this is beneficial to the dynamic stability of concrete blocks that have been disconnected. Due to the fact that they are adequately constructed and sufficiently squeezed on rocky foundations, CFR dams are extremely secure when subjected to seismic stresses.

The security of the dam is not in jeopardy because a conventional two-dimensional dynamic study of the dam's tallest parts predicted that the crack width in the face slab that may occur as a result of considerable dynamic stress and deformations is fairly low. This finding explains why the dam's safety is not in jeopardy. On the other hand, the behavior of the concrete face during a significant earthquake is still not completely understood. This is especially the case when taking into consideration the cross-canyon excitation, which has been ignored due to the intricacy of the phenomenon (Silveira and Pedroso 2018). Large membrane forces created by cross-canyon excitation in the slab may be the source of local bending at the joints, water stops rupturing, and/or rigid body motions of certain slab parts.

In the event that such movements take place, the flow over the slab will much outnumber any leaks that are brought on by structural defects. In addition, joint damage can be caused by three-dimensional dam deformations in narrow valleys, which can be caused by earthquakes that occur in the direction of the valley (and compression and shear stresses in joints).

The height of the CFR dams that are now in the process of being constructed will be increased by more than 200 meters. Seismic activity can cause localized damage to the concrete face, particularly substantial joint displacements, which can greatly increase the quantity of water that seeps through. Seismic activity can also induce cracks in the concrete face. Concerning the safety of dams with an extremely high CFR, it is of the utmost importance to determine whether or not the repercussions of joint leakage (with broad opening) under high hydrostatic pressure are the same as they are when the pressure is low to moderate. This is because the repercussions of joint leakage under low to moderate pressure are the same. Because there have been no reports of significant ground shaking at any of the region's main dams as of this time, the possibilities that have been detailed should be taken with a grain of salt (Varadarajan *et al.* 2006).

The case study for the sliding stability analysis was a standard gravity dam that was made entirely of concrete but did not have an overflow monolith attached to it. Analysis and verification of sensitivity to the coefficients of friction and cohesion are based on the deep stability of the anti-slip sealant foundation system, which is based on these coefficients. This provides the basis for the analysis. Using the Monte Carlo method, a probabilistic seismic test of the gravity dam foundation system is carried out. It will be necessary to conduct analysis on a very large number of samples in order to fulfill the requirements of this evaluation (Liang *et al.* 2020). Utilizing the sliding instability failure mode and the accompanying damage index threshold values makes it possible to do an assessment of the degree of damage that was sustained and provide a conclusion on how severe it was. Ongoing efforts include doing research on seismic fragility analysis and generating seismic fragility curves. Both of these activities, which may be used to the evaluation of a region's susceptibility to earthquakes, are seismic fragility curves and seismic fragility analysis. In order to lay the framework for a probabilistic evaluation of the seismic hazard, a comprehensive examination of the seismic stability of the gravity dam is carried out (Seiphoori *et al.* 2011). Figure 2.5 depicts the geometric characteristics of the sliding block, and Figure 2.6 illustrates the cross section of the dam. Both figures may be found in the same document.

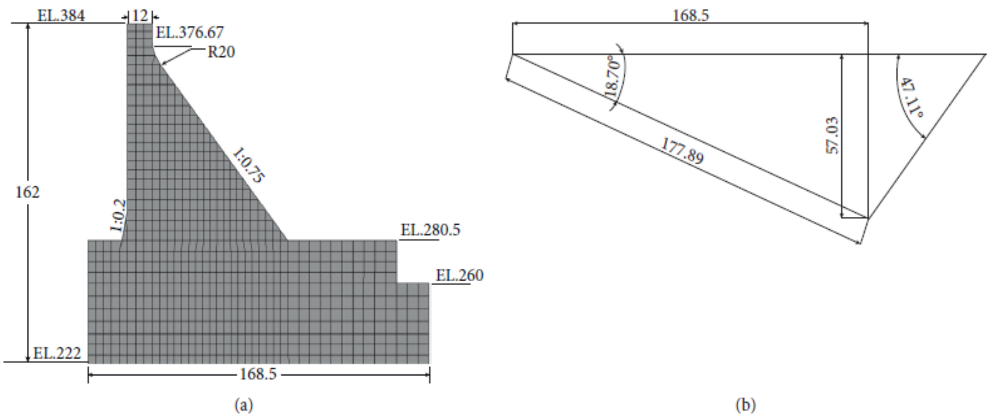

Figure 2.5 **(a)** A description of the standard monolithic gravity dam, which does not allow any overflow **(b)** A description of the block that slides (Liang *et al.* 2020).

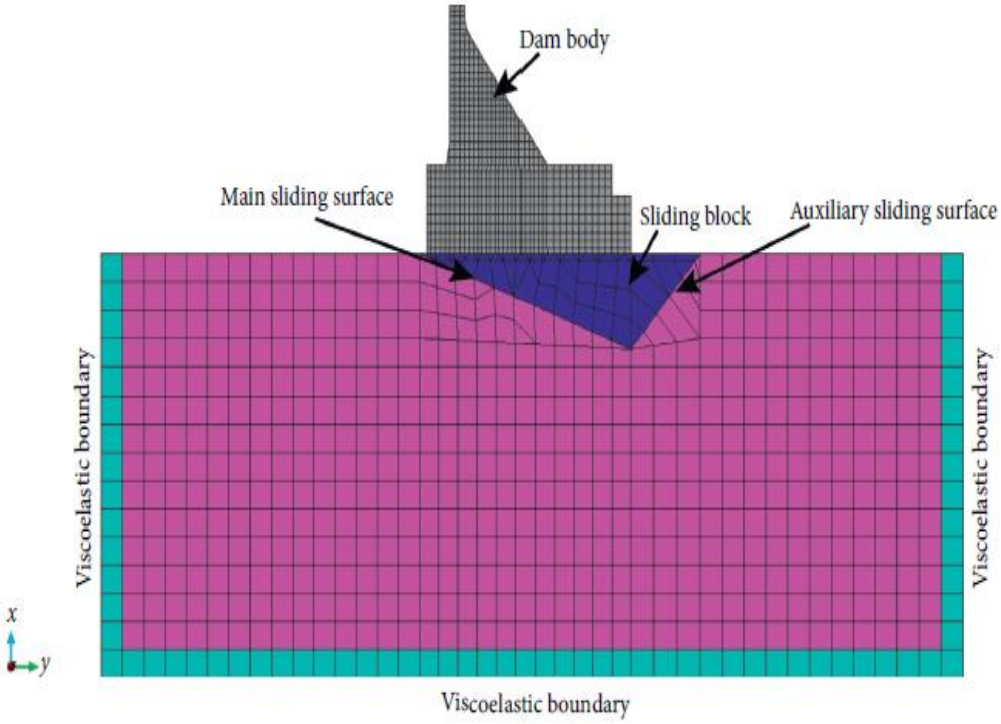

Figure 2.6 A finite element mesh representation of the dam, including the sliding block and reduced borders of the foundation (Liang *et al.* 2020).

The effect that incorrect parameter values have on the shearing slide that takes place on the primary sliding surface may be broken down into three distinct stages, each of which can be recognized independently. This procedure can be divided into three stages, which are the obvious effect before PGA at 0.3 g, the moderate influence between 0.3 g and 0.6 g, and the significant variability after PGA at 0.6 g. The obvious effect comes first, followed by the moderate influence, and then by the significant variability. The model's median and average capacities, in addition to those of the concrete gravity dam, are relatively equivalent to one another. This is also true of the dam's capabilities. Because of the strong correlation between low dispersion and seismic reactivity, the base-case or median/mean model can more accurately predict the median/mean reaction of dam samples than the computer-intensive IDA with LHS can. This is because low dispersion and seismic reactivity have a strong relationship with one another. This is due to the fact that low dispersion and seismic reactivity have a strong positive correlation with one another. Because the base-case model takes into consideration the significant link between low dispersion and seismic reactivity, this is the result. This is the rationale behind why things are the way they are. It's possible that the fact that this is the case can be explained by the fact that insufficient dispersion has a substantial connection with seismic activity.

In addition, the determination of damage thresholds can be carried out utilizing any one of the following procedures: (1) The shear strip that is located on the main sliding surface has a width of forty millimeters, and the width of the drain hole is less than forty percent of the total width of the main sliding surface. As a consequence of the components that were discussed earlier in the sentence, this results in the occurrence of localized slip instability. (2) the overall sliding instability of the concrete gravity dam, as seen by the mean and median values of the IDA curve. This general sliding instability was proved by the dam's failure to hold back water. When constructing seismic fragility curves, the seismic damage thresholds serve as the point of departure for the development of the curves. When utilizing MDE, there is a likelihood of local gravity dam sliding damage of less than ten percent, and there is almost no potential of obtaining wide sliding instability. Even when MCE is incorporated into the design, a gravity dam made of concrete is still able to deliver a substantial amount of sliding stability. Despite the fact that the model that was used can only simulate a single concrete gravity dam and does not take into consideration all of the uncertainties and nonlinearities that may be present, the findings are significant and have the potential to serve as a basis for further investigation. This is the case despite the fact that the model that was used can only simulate a single concrete gravity dam. In addition to this, the following characteristics may be taken into consideration: (1) the fluctuation from one record to the next; (2) the relationship between the several components of sliding; and (3) the nonlinear behavior of the material (Engel *et al.* 2014). The 27 CFRD case studies that were made available are going to be utilized in this article to describe post-construction leakage and deformation. Figure 2.7 provides a visual representation of the zone names that apply to a concrete face rockfill dam (CFRD) that has sound rockfill. When the height of the dam is greater than one hundred meters, certain designations come into play. The long-term leakage rate begins to grow at an accelerated pace after the height of the dam is larger than 125 meters, and the deformation that is normal to the face slab becomes greater than the post-construction crest settlement at this point (Won and Kim 2008).

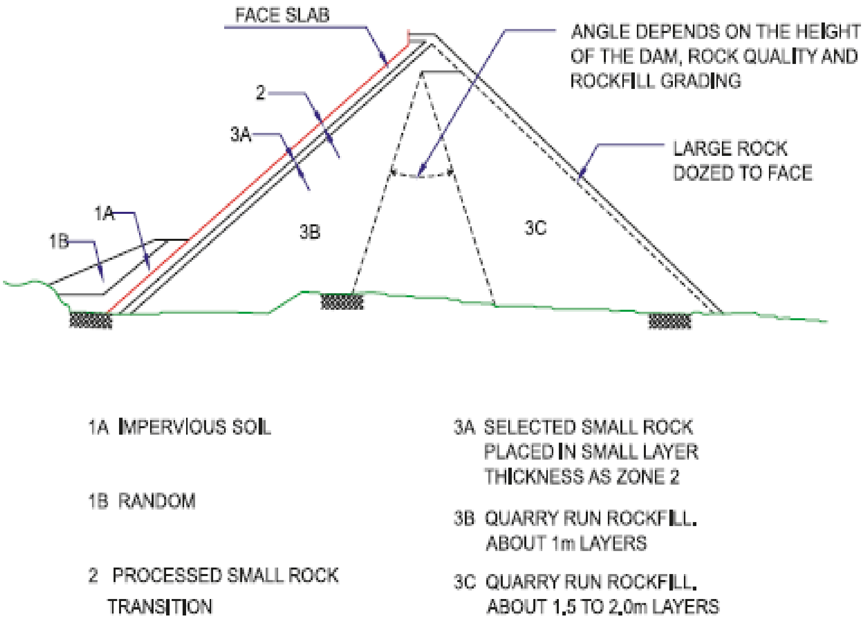

Figure 2.7 Zone designs for concrete face rockfill dam (Won and Kim 2008)

They came to the conclusion that the initial filling of the water load does not have any impact on the normal face slab crest settling or deformation that occurs after construction. The process of filling was responsible for the vast majority of the normal face slab's distortion.

The range of post-construction crest settlement showed substantial agreement in cases in which very high intact strength rockfill was utilized; however, it tended to underestimate crest settlement in cases in which medium to high intact strength rockfill was used. The amount of the crest settling that occurs over the long period after construction is comparable to the deformation that occurs normal to the face slab.

When the height of the dam is less than 100 meters, the crest settlement is more than the deformation that is normal to the face slab, but when the height of the dam is greater than 100 meters, the crest settlement is decreased. Because of the weight of the water on the first filling, the areas of the slab that are closest to the crest and toe of the concrete face slab, respectively, experience the highest levels of compressive and tensile strains. The long-term leakage rate is less than 10 liters per second (L/s) when the height of the dam is less than 122 meters, but it soon increases to 45–200 L/s when the height of the dam is greater than 125 meters (Ariyan *et al.* 2016)

A similar quasi-continuum model for the percolation of crack-intensive sides was used in the calculation of the permeability coefficient of a concrete slab rockfill dam (CFRD). This helped in the creation of a finite element model and improved the computation of dam seepage. Furthermore, technologies such as particle swarm optimization and support vector machine inversion were developed and put into use. Figure 2.8 depicts the typical approach taken when analyzing seepage. It has been shown (Shi *et al.* 2019).

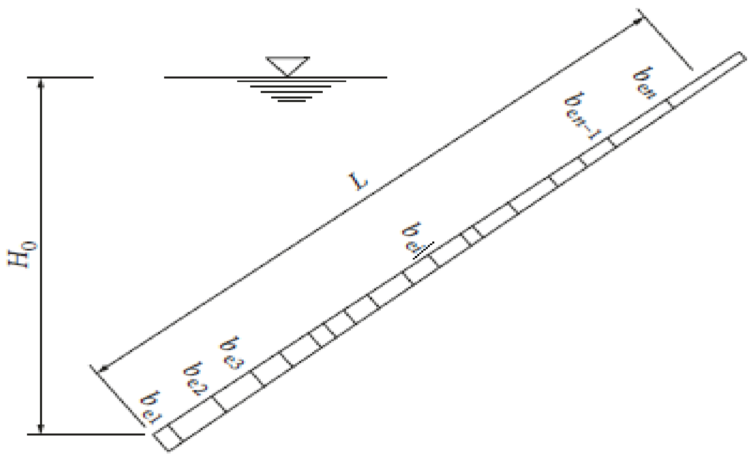

Figure 2.8 Seepage analysis model (Shi *et al.* 2019)

The depth of the area analyzed on a fundamental level was determined to be 120 meters. In this particular analysis, it was determined that the undrained boundary would act as the intercepting boundary. Figure 2.9 illustrates the finite element model of the CFRD.

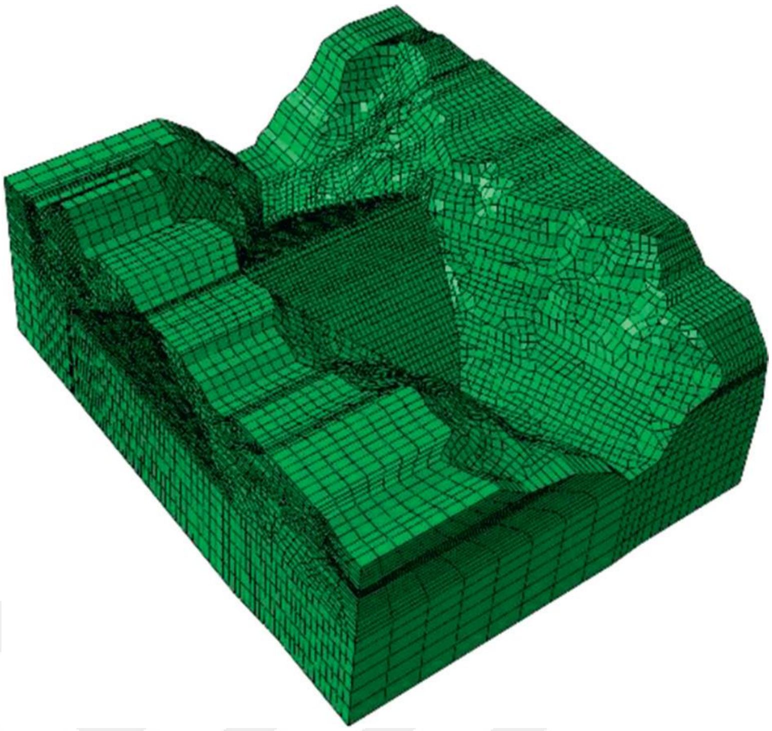

Figure 2.9 Finite element model of CFRD (Shi *et al.* 2019)

They discovered that because the CFRD is thicker and stiffer than the cushion, various types of fractures may appear on its face during manufacturing or storage, jeopardizing the anti-seepage system. Given the importance of concrete slabs in the CFRD's anti-seepage system, which simplifies finite element model construction and boosts computing efficiency. In the process of inverting the permeability coefficient, the PSO-SVM inversion technique functioned successfully when monitoring data was used. Seepage discharge was calculated using the coefficients from the two different methodologies, and the results were extremely similar to the monitoring data, which suggests that both approaches are beneficial and applicable in real-world situations. This paper provides the groundwork for future research into the seepage aspects of CFRD fractures and is therefore extremely important.

Regional seepage discharge measurement, on the other hand, can help with identifying the accurate discharge at each part, ensuring safe monitor operation, narrowing the search range for accidents in an emergency, avoiding blindness, and facilitating testing of the anti-seepage effect on both banks, the water stop effect of peripheral joints, and the working conditions of concrete slabs. All of these benefits can be achieved by reducing the search range, narrowing the search range for accidents in an emergency, avoiding blindness, and avoiding blindness.

2.3 Concrete Enhancement to Resist Cracking

Minimizing the presence of the flaws described above in concrete in order to improve both its functionality and its appearance Shrinkage cracking is also reduced when fibers are included into the material. The material that made up the fiber was polypropylene. There are many different uses for the synthetic fiber known as polypropylene fiber, which consists approximately 85 percent propylene. Fiber Reinforced The term "Polypropylene Concrete" refers to a brand-new category of building material that is distinguished by its high levels of mechanical strength and stiffness in addition to its exceptional longevity. Many different types of businesses make use of it (Ravishankar and Jeevanantham 2021).

Compression strength tests on cubes were performed seven and 28 days after the cement had cured, with varying percentages of mixed polypropylene being added to the weight of the cement. The results of the compressive testing may be seen in Table 2.1.

Table 2.1 Compressive strength of concrete

SPECIMEN NO.	PROPORTIONAL	7 DAYS	28 DAYS
1	Conventional	23.25	32.58
2	0.4%	16.62	29.18
3	0.6%	23.99	34.66
4	0.8%	25.62	37.62
5	1.0%	23.25	32.29

They observed that polypropylene fibers, due to their flexibility and ability to bend to shape, reduce the quantity of plastic shrinkage fractures (Yadav *et al.* 2017). The inclusion of 0.1 percent fibers by volume has been proven to reduce cracking by a factor of 5 to 10%. The extent of fracture reduction is determined by the fiber content of the concrete. However, I'm looking at M30 concrete at this point in the project. Each series is made up of cubes, cylinders, and prisms, according to the IS standard. A battery of tests was done at 28 days to measure compressive strength.

In 2012, Behfarnia and Sayah (2012) using the finite element analysis program ABAQUS, To verify the effects of fibre-reinforced plastic (FRP), a non-linear static analysis was performed on the maximum bearing capacity of concrete shear water flows from the holes. To ensure that the numerical model was correct, the results of an experimental and numerical study of a concrete shear water flow were compared. The effects of producing cut-off apertures as well as the strengthening effects of adding FRP were explored after the Finite Element Model (FEM) was confirmed.

With an upper and lower dam linked monolithically, the water flow was 750 mm broad, 750 mm high, and 70 mm thick. Figure 2.10 and Figure 2.11 shows the top dam test arrangement (1150mm long, 150mm deep, and 200mm thick) (Behfarnia and Sayah 2012).

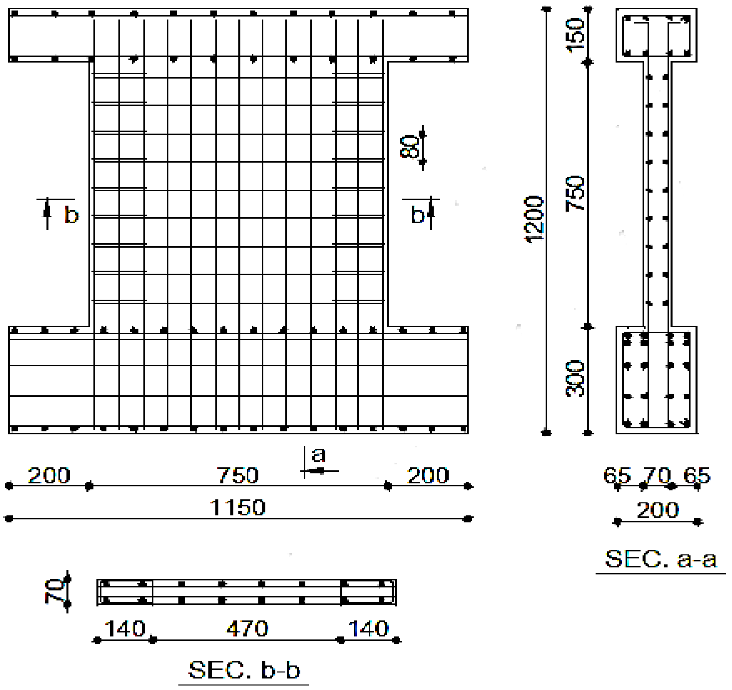

Figure 2.10 Rebar details and water flow dimensions (mm) (Behfarnia and Sayah 2012)

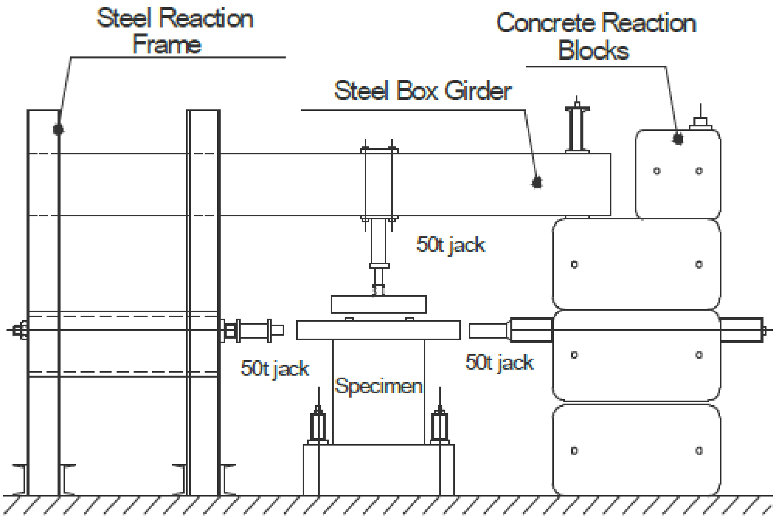

Figure 2.11 Test setup (Behfarnia and Sayah 2012)

The top and bottom portions of the aperture, each having a width of Y1/2 (Y1 being the opening height), are wrapped in unidirectional carbon fiber reinforced plastic (CFRP) with the fibers aligned horizontally, and the reinforcing approach makes use of two piers. According to the diagram, the thicknesses C1, C2, and C3 of the CFRP employed to reinforce shear water flows are similar to 0.05, 0.08, and 0.12 mm, respectively (Figure 2.12)

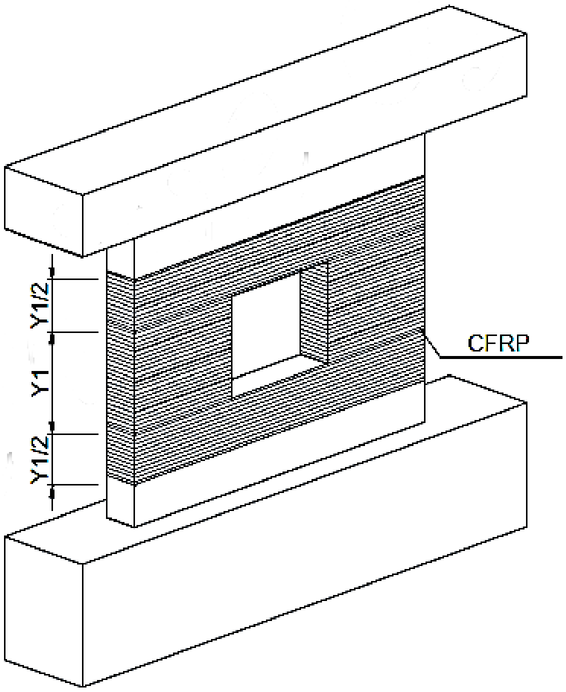

Figure 2.12 CFRP scheme used as external strengthening (Behfarnia and Sayah 2012)

The capacity of the finite element approach technique to offer a realistic forecast for the behavior of RC shear water flows was demonstrated through a comparison of experimental and numerical data. The comparison was carried out to demonstrate the capability of the procedure. When apertures made up 11.11 percent or less of the overall water flow area, the load capacity was lowered by 37.1 percent.

The failure of RC shear water flows with apertures that disturbed the load channel was mostly caused by the size and positioning of the holes, which played a significant part in the failure. When the opening area is extended to 25 percent (a big aperture), the capacity reduces by 61.9 percent. This is because more of the total area of water flows through the opening. In addition, adjusting the orifice position relative to the height of the water flows in the large aperture models had no discernible impact on the maximum load capacity of the water flow. This was the case even if the maximum load capacity was increased. Because of the opening, the integrity of the shear water flows was transformed into a frame action. This meant that the overturning moments were primarily resisted by an axial compression–tension connection throughout the water flow system rather than by the individual flexural action of the water flows.

Depending on the size and location of the aperture, shear strengthening around RC shear water flows has the potential to significantly improve the water flow capacity. The increase in capacity given by FRP sheets ranged from 1% to 39%. The capacity improvement was at its maximum point when the aperture was operating at the point where the water flow was at its highest point. The water flows that had bottom apertures only showed a 6% boost in their strength.

Failures of reinforced and un-strengthened RC shear water flows with apertures were impacted by the thickness of the FRP, as well as the positioning and size of holes. Increasing the thickness of the CFRP plate would result in an increase in both the ultimate load and the displacement associated with it in models with large apertures. On the other hand, in models with smaller apertures, increasing the thickness of the CFRP plate would significantly increase the displacement associated with the ultimate load.

Using three tiny high-strength concrete slabs, researchers investigated the effect of adding steel fiber on ultimate punching strength. Figure 2.13 shows the slabs, which were 500 mm square and 60 mm thick (Arna'ot *et al.* 2017).

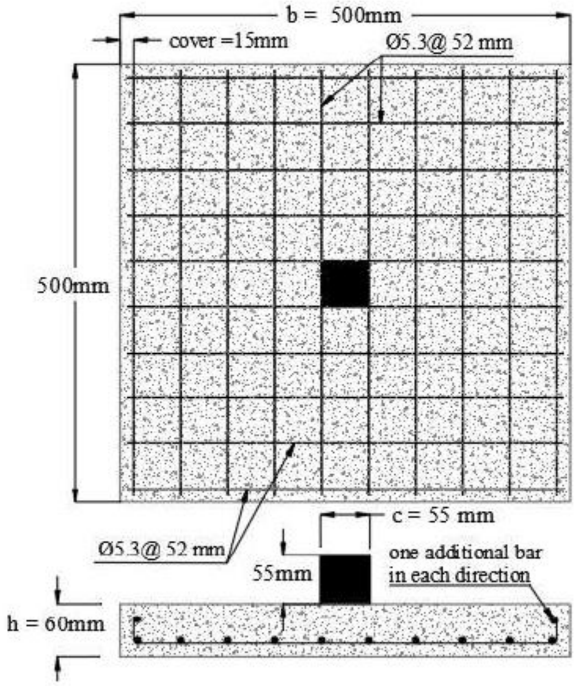

Figure 2.13 Slab geometry (Arna'ot *et al.* 2017)

The slabs were 500 mm square and 60 mm thick, with two steel fiber doses of 0.75 percent and 1.25 percent, as well as traditional reinforcing bars of moderate ratio.

The researchers found that incorporating 1.25 percent steel fiber by volume of concrete increased ultimate punching shear resistance by 17 percent when compared to plain concrete slabs, but this effect was less than on low strength concrete slabs. Steel fiber also reduces deformation caused by different load stages and reduces the diameter of critical shear cracks. There were no impacts on the inclination of the punching shear fractures for two steel fiber percentages.

All of the slabs tested demonstrated punching failure, however, the slabs had a slight horizontal plateau before achieving the ultimate load displacement.

An investigation was conducted to determine whether or not it would be possible to use recycled PET bottles as a partial replacement agent for fine aggregate in concrete. The performance of concrete mixtures that contained 1%, 2%, and 3% of PET bottle fibers as a replacement for fine aggregate was evaluated and compared to the performance of control mixtures that had no such substitute (Lasiyal *et al.* 2016).

To determine the replacement percentage, a percentage of the proportioned mixture's total fine aggregate content is used as the basis for the calculation. In order to make a comparison with a control mixture, cube specimens with dimensions of 100 millimeters by 100 millimeters by 100 millimeters, cylinder specimens with dimensions of 150 millimeters in diameter and 300 millimeters in height, and prism specimens with dimensions of 100 millimeters by 100 millimeters by 500 millimeters will be cast in PET bottles that have been grounded. On hardened concrete, compression, flexural, and split tensile tests should be carried out after 7, 14, 28, and 56 days have passed since the concrete was placed (Lasiyal *et al.* 2016).

When PET bottle flakes were used in lieu of fine aggregate, it was discovered that the compressive strength of the fine aggregate decreased by up to 2 percent, and when PET bottle flakes were used in place of coarse aggregate, it decreased by up to 3 percent. As a direct result of this, it will be fair to replace the fine aggregate with 2% replacement. Flexural strength decreased by 2 percent immediately after fine aggregate was replaced with PET bottle fibers, and then it decreased by 3 percent after some time had passed. As a result, it won't be unreasonable to replace fine aggregate with two percent of the replacement material. The split tensile strength of the material dropped by up to 2 percent when fine aggregate was replaced with PET bottle flakes and by up to 3 percent when fine aggregate was replaced with PET bottle flakes. The substitution of the fine aggregate with two percent of the total volume will provide a split tensile strength that is adequate when measured against the other specimens that were cast and examined. Because of this, replacing the fine aggregate with two percent flakes made from PET bottles will be significantly more acceptable than other replacement percentages such as one percent and three percent. This is due to the fact that the compression, flexural, and split tensile strengths will all be significantly reduced when the fine aggregate is replaced. According to the findings of research, replacing 2% of the fine aggregate with coarse aggregate led to a reduction in the amount of strength lost while also leading to a cost savings of Rs 9.5 per cubic meter of concrete. It is feasible to change mortar with plastic fibers into light weight concrete based on unit weight since the weight of the concrete made with PET fibers was lowered.

Plastic concrete materials were used in a study to estimate a suitable plastic concrete mixing design for cutoff water flows to prevent leakage beneath the earth dam. This was accomplished by adding a specific amount of clay (Betonite) to the plastic concrete materials, which lowered the concrete's hardness and elasticity coefficient (Pashazadeh and Chekani-Azar 2011).

To reduce the risk of hydraulic failure and cracking, Ebonite (clay and excavation mud) is used. Analyzes the plastic components of concrete as well as aspects that impact its characteristics and mixing design. Figure 2.14 shows a concept for a plastic concrete mix.

Parameters characteristics obtained from tests					**Material amount used in Plastic concrete mixing plan**				
Dam name	$f_c(\frac{kg}{cm^2})$	$E_c(\frac{kg}{cm^2})$	Slump (cm)	$K(\frac{m}{sec})10^{-10}$	gravel	sand	cement	Bentonite	water
Stor	19.0	42500	21	7.4	850	750	36	150	450
Arasbaran	8.5	-	-	4.5	800	700	50	110	400
Karkhe	31	37000	19	4.7	795	705	37	195	360
UKAI	-	-	-	-	100	740	0	210	970
Salman farci	44.44	7300	-	-	990	810	60	180	350
Khalf abad	-	-	-	-	750	750	50	150	350
Shahrchay	-	-	-	-	850	850	60	140	400
Tehtali	5.8	-	-	-	400	650	48	200	600

Figure 2.14 Sample of plastic concrete mix design

The graphs and correlations shown in this paper may be used to determine the ratio of adhesive materials to the amount of water used in plastic concrete, allowing cutoffs to be designed with time and money saved. In certain circumstances, achieving optimum conditions is difficult, if not impossible. We need to figure out how to limit features and qualities more effectively.

Numerical analyses of the dependent variables (fc, E, and K) and independent factors (B, W/B, W/C) in the presented diagrams demonstrate a strong correlation ($R>0.6$) based on actual experiences. The most effective components appear to be accuracy, inability to measure changeable parameters, and lack of adequate precision in determining the characteristics and variable nature of the parameters under study.

The effect of HDPE plastic fibers on the performance of concrete was studied. One method for decreasing this type of waste is to incorporate it into concrete. We investigated how HDPE-type polymers may be used as a 14 material to improve concrete's hardness, tensile strength, and 15 compressive strength (Rahman and Nurdiana 2020).

They evaluated a total of 156 samples to determine the effect that HDPE plastic fibers had on 16 different grades of concrete, ranging from B0 (the lowest quality) to f'c25 MPa (the highest quality) (medium and high quality).

In addition, each of the 18 grades of cement was mixed with one of 17 different HDPE plastic fiber compositions (2.5 percent, 5 percent, 10 percent, and 20 percent by weight of cement), with HDPE plastic fiber diameters of 1 x 1 centimeters, 0.5 x 2 centimeters, or 0.25 x 4 centimeters, as shown in Figure 2.15.

Figure 2.15 The preparation of high-density polyethylene (HDPE) plastic fibers, including **(a)** the preparation for the cutting process and instruments, and **(b)** HDPE 192 fibers with a size of 0.5 x 2 cm (Rahman and Nurdiana 2020)

According to the findings of this experiment, the optimal percentage of HDPE plastic fiber to add was 5 percent, and the cross-sectional form of the fiber should be 0.5 cm by 2 cm. The tensile strength of fibers measuring 1 x 1 centimeter and 0.25 x 4 centimeter only increased by 10 percent and 5 percent, respectively, over the previous iteration. What happens to the HDPE fibers in f'c10 MPa concrete when the concrete breaks apart as a result of stress is seen in Figure 2.16 below.

Figure 2.16 Visualization of the state of the HDPE fibers: **(a)** 1 centimeter by 1 centimeter, **(b)** 0.5 centimeters by 2 centimeters, and **(c)** 0.25 centimeters by 4 centimeters (Rahman and Nurdiana 2020)

They also found that using HDPE plastic fibers as a concrete addition material may increase the composition's strength, and that this improvement can be achieved by adding 5 percent HDPE to all different diameters of fiber. The f'c10 MPa concrete quality was found to demonstrate the best interaction with the additional HDPE plastic fiber material out of the three different concrete qualities that were tested. They also came to the conclusion that extra HDPE plastic should only be used on concrete of poor quality and that which is not structural.

It is advised to add between 5 and 10 percent of HDPE plastic fibers to concrete when constructing water flow panels from precast concrete with a ten-megapascal compressive strength (f'c10 MPa). There is a need for more study to establish the consequences of combining more than 20 percent HDPE and other types of plastics with concrete, including the affect on thermal insulation (Nurdiana 2021, Appiah *et al.* 2017).

The purpose of this study was to determine the ideal ratio of HDPE plastic fiber to concrete, which can then be applied in construction. These discoveries will assist to improve easy-moving weight concrete for environmentally friendly structures, particularly in situations involving non-515 structural concrete. In addition, the utilization of HDPE fibers may result in the development of waste reduction strategies that are less detrimental to the environment.

An orthogonal experimental approach is used to analyze 30 batches of samples with varying indicators in terms of volume percentage and width to height ratio to strengthen the fibers and to determine the best part of the hybrid fibers in terms of Peak strain and compressive strength where analysis of variance is used. This was done while the reinforced concrete with hybrid fibers made of polypropylene and steel was being examined under uniaxial pressure (HFRC). The preparation of prism specimens with dimensions of 150 mm x 150 mm x 300 mm for the uniaxial compression test is illustrated in Figure 2.17 (Chi*et al.* 2014).

Figure 2.17 Testing system (Chi *et al.* 2014)

3. METHODOLOGY

3.1 Introduction

For numerical study, the FEM was created in ANSYS Finite Element to simulate the forces acting on the panels. The finite element method (FEM) is widely used in civil engineering and other fields of technology as a kind of numerical analysis (Mohammadi 2008). This chapter discusses how the HDPE content of the concrete was estimated, as well as how laboratory data was entered into ANSYS so that panel performance could be evaluated at a variety of temperatures. This article will explore how similar panel operations may be achieved. It is possible for the panel to be subjected to a broad variety of loads; this will depend on the size of the panel as well as the reinforcements that are utilized. Defining how to explain the need for panel data is the most difficult part of this technique. The panel component was built with experimental data, and the model was verified with the same data. Once the question is answered, the protection equations can be derived. In the simulation method, all lengths and volumes are expressed in metric (Li *et al.* 2020). The mechanical features of the model, such as their sensitivity to changes in loading level, were investigated through simulation studies to identify the most influential components. The primary objective of this research is to develop a numerical model that is able to predict the characteristics of panel displacements, including HDPE's, when they are subjected to high temperatures, and then to compare those results to those obtained by studying the behavior of regular concrete with the same panel dimensions. In addition, one of the secondary goals of this research is to determine whether or not the HDPE's are able to withstand the high temperatures that are predicted by the model.

3.2 Developing the Model

Both HDPE and cement kinds produced locally were utilized in the binding procedure. Sand was used as the fine aggregate, and the quantities were adjusted correspondingly. To study how HDPE impacts the performance of concrete, the researcher conducts laboratory tests. Table 3.1 and Table 3.2, respectively, detail the physical and chemical properties of HDPE (Nurdiana 2021, Chowdhury and Hossain 2020).

Table 3.1 Physical properties of HDPE (Nurdiana 2021)

Sr. No.	Properties	Test Results
1	Compressive strength at 28 days, N/mm^2	92%
2	Drying shrinkage (%) max	0.10
3	Particle shape	Spherical
4	Colour	Grayish white
5	Specific gravity	1.8-2.4

Table 3.2 Chemical properties of HDPE

Sr. No.	Properties	Test Results
1	SiO_2+Al_2O_3+Fe_2O_3 (%)	93.0
2	SiO_2 (%)	77.0
3	MgO (%)	0.9
4	SO_3 (%)	2.2
5	Na_2O (%)	0.8
6	Loss on ignition (LOI) (%)	5.0
7	Total chlorides, % by mass index	0.05

In this study, 20mm crushed basalt was used as coarse aggregate. When used as a partial cement replacement, the effect of pozzolanic polymers like HDPE on concrete quality can be exploited to gauge concrete performance. We came up with two different HDPE and concrete blends. Both high-density polyethylene (HDPE) and concrete were made from the blended cement. Mix A, which is HDPE-free, stands in for regular concrete, while Mix B, which is HDPE-heavy, is an extreme contrast (Mix B). The proportions of the concrete mix are summarized in Table 3.3 (Achilleos *et al.* 2011, Mohod 2015).

Table 3.3 The mix design

Mix Code	Content	V_f %	Cement (KG)	Sand (KG)	Gravel (KG)	Water (KG)	Silica Fume (KG)
MixA	None	0	10.0	26.5	17	3.5	0.8
MixB	Ash	0.70	7	26.5	17	3.5	0.8

- In this investigation, cement produced from Kubaisa and obtained from western Iraq was utilized.

- A consistent percentage of a water reducer with a high water content is added to all combinations since the anticipated combination's workability is too poor. The standard Sika superplasticizer that conforms to ASTM C 494 Types A and B is utilized (Khayoun *et al.* 2020).
- The fine aggregate is screened river sand sourced locally. The sizes of the used particles ranged from 0.075% to 4.755% of a millimeter.
- The coarse aggregate consists of crushed stone with a particular size gap grading. Even coarse aggregate contains a greater proportion of fine aggregate, as indicated by the difference between the largest particle size (9.5 mm) and the next largest particle size (3.5 mm) (4.75 mm).
- HDPE is produced as a heterogeneous byproduct when coal is burnt in power plants. A fine gray powder composed of spherical glass particles rises with the exhaust gases. Due to the presence of pozzolanic components, HDPE can be combined with lime to produce cementitious materials. As seen in Figure 3.1, HDPE is utilized in a variety of environments, including concrete, mines, landfills, and dams.

Figure 3.1 HDPE samples

Particles in the condensed silica fume are typically round and have a diameter of around 150 nanometers. Silicon, iron alloys, and silicon itself are all byproducts in the manufacture of this amorphous substance. We utilised water in the concrete mixing and curing processes throughout the duration of the project.

Beginning the curing phase, the sample was heated to 25 degrees Celsius in a water tank for 28 days (Figure 3.2)

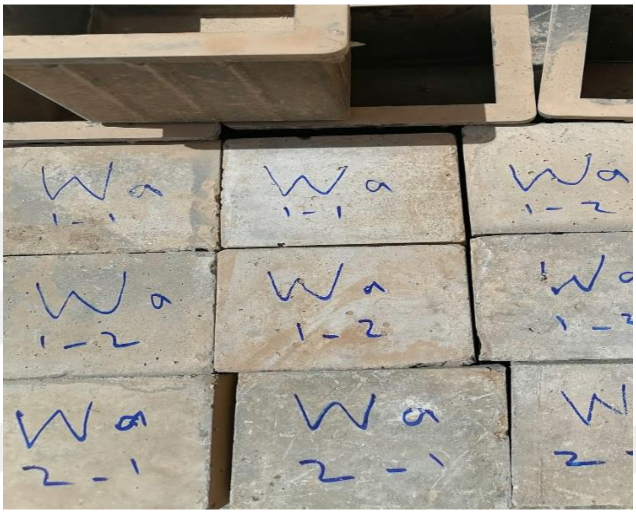

Figure 3.2 The samples after curing phase

Mechanical properties of concrete

The testing of Cubic and the panel took place on the same day. Figure 3.3 depicts the apparatus used for all cubic tests.

Figure 3.3 Test machine

Compressive process

The procedure for determining the compressive strength of cubic concrete specimens is outlined (ASTM C39, 1997). The sample is put in the machine's crest (Figure 3.4).

Figure 3.4 Test process

3.3 The ANSYS Process

The shape of the gadget based on human input (IGS files). This approach generates a panel containing a collection of points and lines that can be used with a 2D drawing before going on to the geometry step. This drawing is comprised of points, lines, arcs, and conic sections. The following are the geometry creation steps in SolidWorks:

For each type of panel in SolidWorks, choose a (Part File). The researcher used a variety of panel types and thicknesses to illustrate the effect of panel form design.

In the following phase, all of the information gathered thus far will be imported into SolidWorks by making use of the program's features. The next step is to input the panel's dimensions into the SolidWorks program. The connection between the points in a section specifies the radius of curvature of the surface. The geometry of the panel's base form will be used to design the panel's components, which will be used in the preliminary simulation phase to study the panel's force responses.

Third, save the geometry with an IGS file extension.

3.4 Pre-Process Steps

The research expenditure will vary based on the criteria and objectives of the investigation. Ensure that all data utilized to set parameters and objectives comes from the same source as a matter of first importance in any research project. We then explain the next steps (Jagota *et al.* 2013, Panfilov *et al.* 2020):

3.4.1 Geometric data specification

Studying the panel model begins with setting the panel and other component settings. Accurately simulating a model's behavior is essential for getting useful results from the simulation method. Here are the basic procedures involved in running an ANSYS simulation:

Each vector controls a distinct component of the model's responsiveness to external forces. During this phase of the process, while the 3D model is being assessed, numerous model iterations are feasible (Figure 3.5) (It was assumed that steel was used to create the sample, and the panel's contents were tested accordingly) (Zienkiewicz *et al.* 2005).

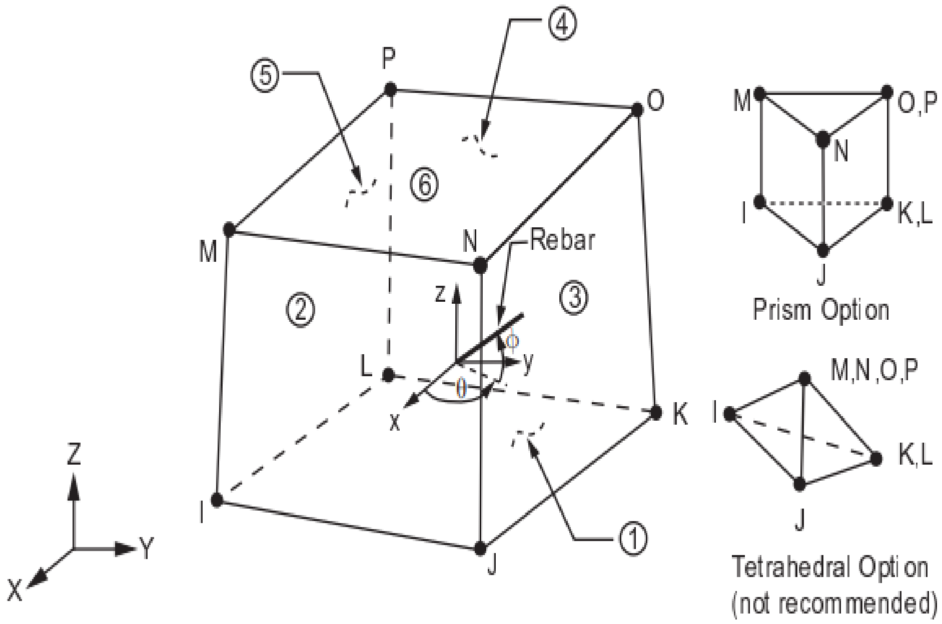

Figure 3.5 ANSYS finite element

Table 3.4 for hard panel materials is where you'll insert the information and industrial qualifications for the supplementary panel, such as tensile stress, transmission coefficients, and compressive principles.

Table 3.4 Material options

Mechanical Properties	**Symbol**	**Steel**
Young's modulus (Gpa)	*E*	207.0
Shear Modulus (Gpa)	*G*	80.0
Poisson's ratio	*V*	0.3
Density (kg/m^3)	P	7600
Yield strength (Mpa)	S_y	370
Shear strength (Mpa)	S_s	370

The success of the entire study is contingent on the user's ability to distinguish between simplifications and the "genuine thing," as well as the mesh and type of element to be deployed. Preprocessing includes both the development of the model and the specification of how it will be loaded. The processor's integrated graphics package enables the creation and display of a virtual representation of the assessed component. The creation of an input file for storing data collected from the pre-geometrical processor and other sources. The material of the model must also have the appropriate mechanical or physical properties, and loads and maybe specific limits on the mobility of individual nodes must be applied (restraints). In the input file, it may be essential to include extra information about the analysis method and the desired output (results), such as whether stresses are to be estimated everywhere in the model, which would save time and money, or only in a subset of the model. Following the completion of the input file, it is transmitted for analysis. If the model is sufficiently simple, the input file can be generated without a pre-processor. If the software permits, the pre-processor may also be able to import geometry data from a CAD (computer-aided design) program for the model. The following considerations are necessary:

1. Developing geometry

The first step in examining the dam model is to specify the features of the concrete and other components. It is an indispensable tool in the simulation toolbox for producing reliable findings of model behavior. Here are the steps that make up the ANSYS procedure:

The first stage involves creating the geometry of the dam.

The degrees of freedom (DOFs) at this point are indicative of the range of motion you may expect it to have due to the applied loads. More than that, though, DOF demonstrates the propagation of forces and timespans from one component to the next. Geometry of a model's nodes and parts are determined throughout the model generation process. One of the most important features of ANSYS is the node, which is a coordinate point in a field where degrees of freedom (DOF) are given. Finite element analysis's second part is the elements themselves, the analysis's building blocks. Each node's DOF is related to the next node's DOF via a mathematical connection. The sizes and shapes of elements vary greatly. Among these are lines, areas (both flat and curved), and solids (both two and three dimensions) (bricks). Modeling techniques available inside the ANSYS software package are as follows:

2. Types of elements

Here, the three-dimensional model is assessed after several possibilities have contributed to its development, which may involve one or more materials. The inputs are analyzed with the assumption that the concrete recipe calls for a given quantity of sand, gravel, and cement. To examine the impact of compositional variation on the material's behavior, more glass fibers of differing quality are added in varying numbers and ratios. The model's effect on forces varies according to the direction and magnitude of three vectors that make up the model. Pictured as in Figure 3.6, Figure 3.7 and Figure 3.8.

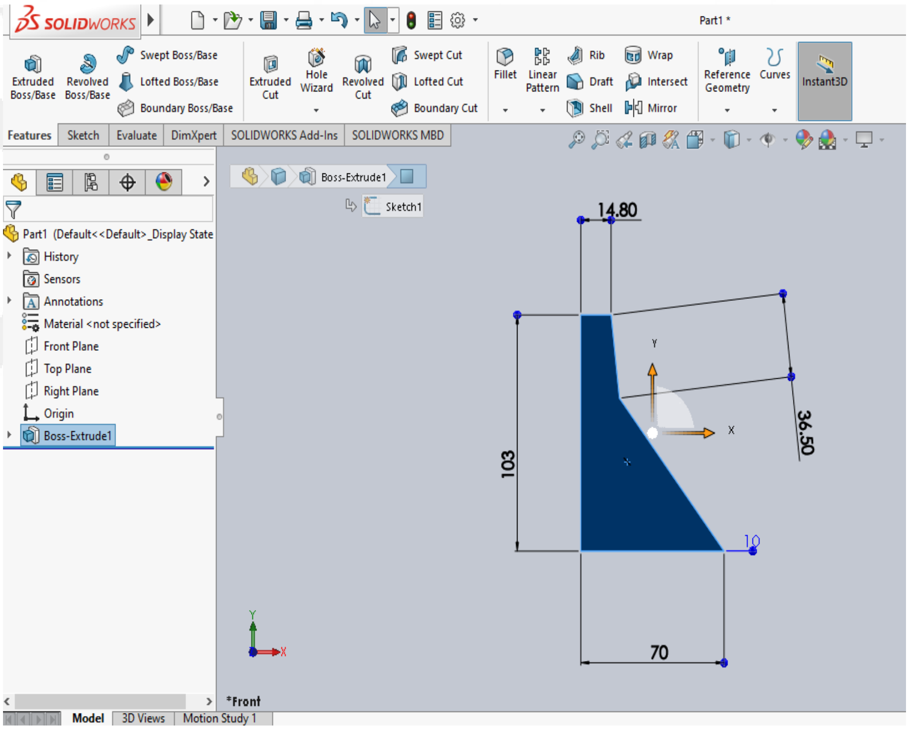

Figure 3.6 The first case of study

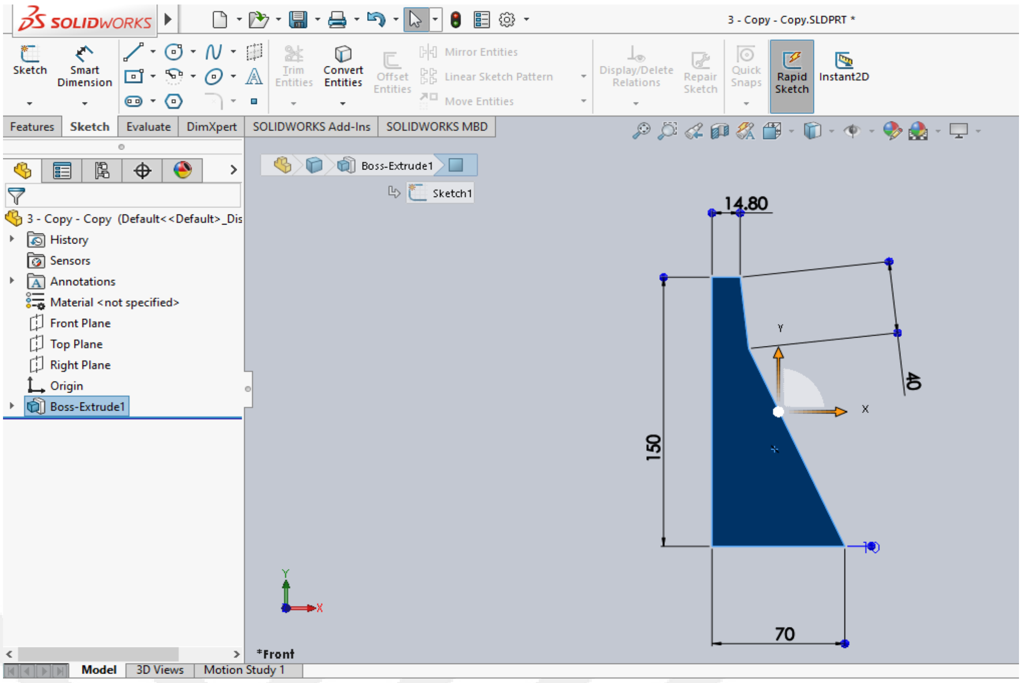

Figure 3.7 The second case study

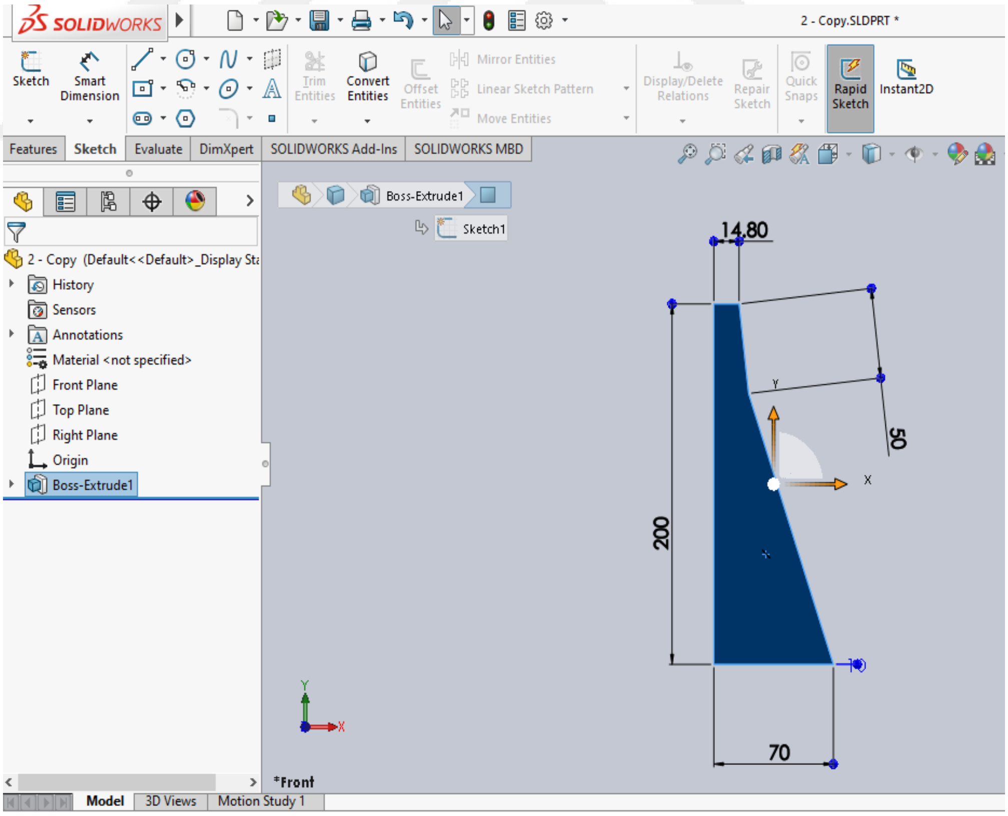

Figure 3.8 The third case study

The ANSYS relationship of sensible model performance is shown in Figure 3.9 and Figure 3.10.

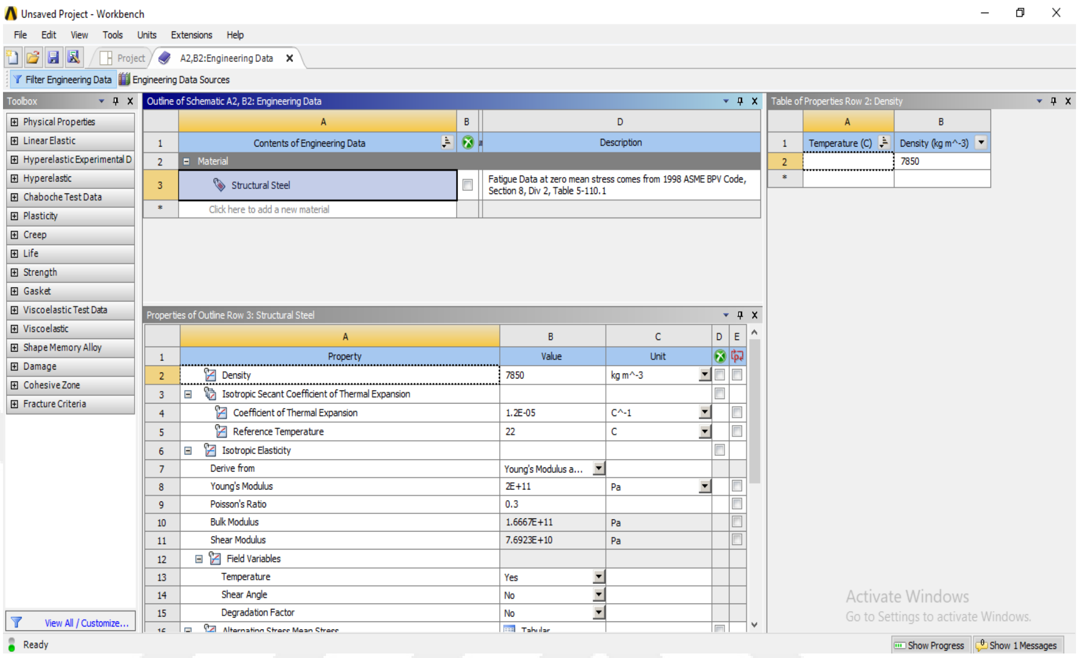

Figure 3.9 Simulation parameters values

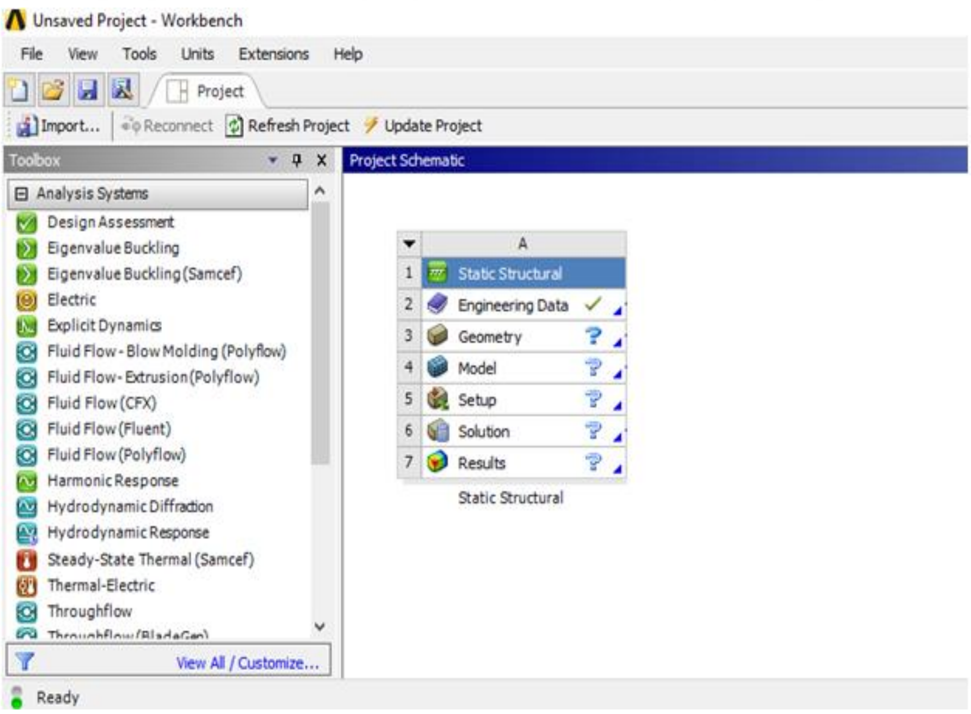

Figure 3.10 Configuration of main ANSYS applied programs

3. Import geometry

All the concrete, rebar, and other additional materials required for the structure's study could be accounted for in ANSYS by inserting them in the mold in the same manner as depicted in the images. This method can be used to enter the values of concrete properties and analyze their response to various loads. To include a model into the ANSYS program, multiple procedures are required. The material data specification can be introduced after the definition of the inserted data from the system-connected model geometry (Figure 3.11) (Figure 3.12) (Figure 3.13). For this model, we begin with concrete, add steel bars to hold the concrete in place, and then use water to exert pressure on the dam.

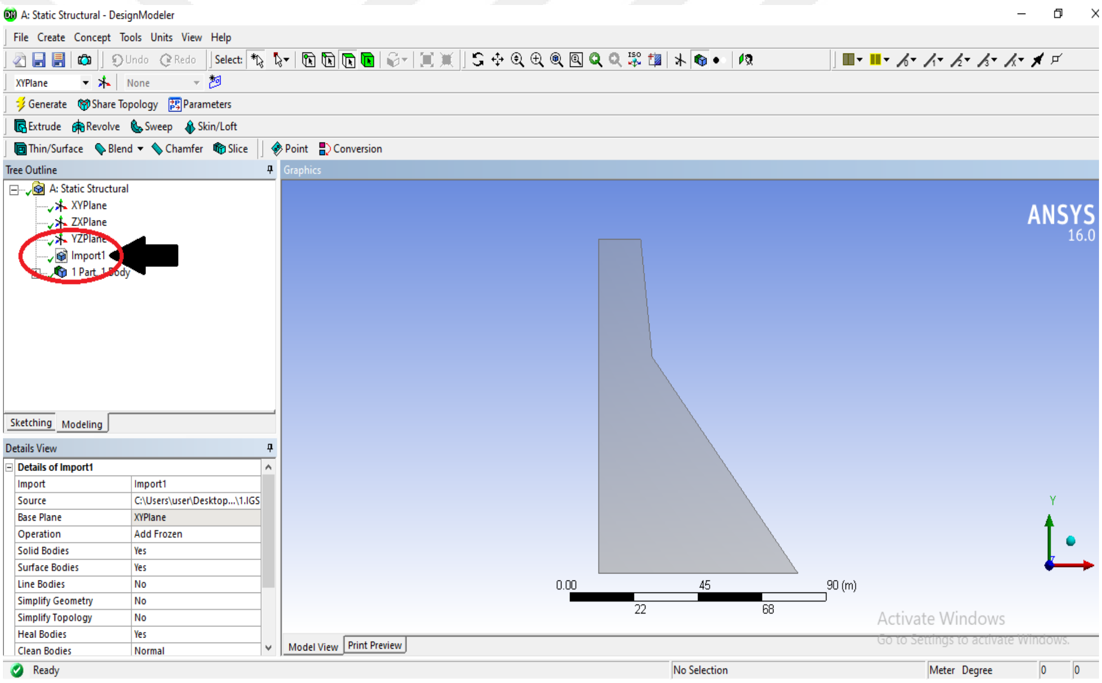

Figure 3.11 Import the dam geometry for first case of study

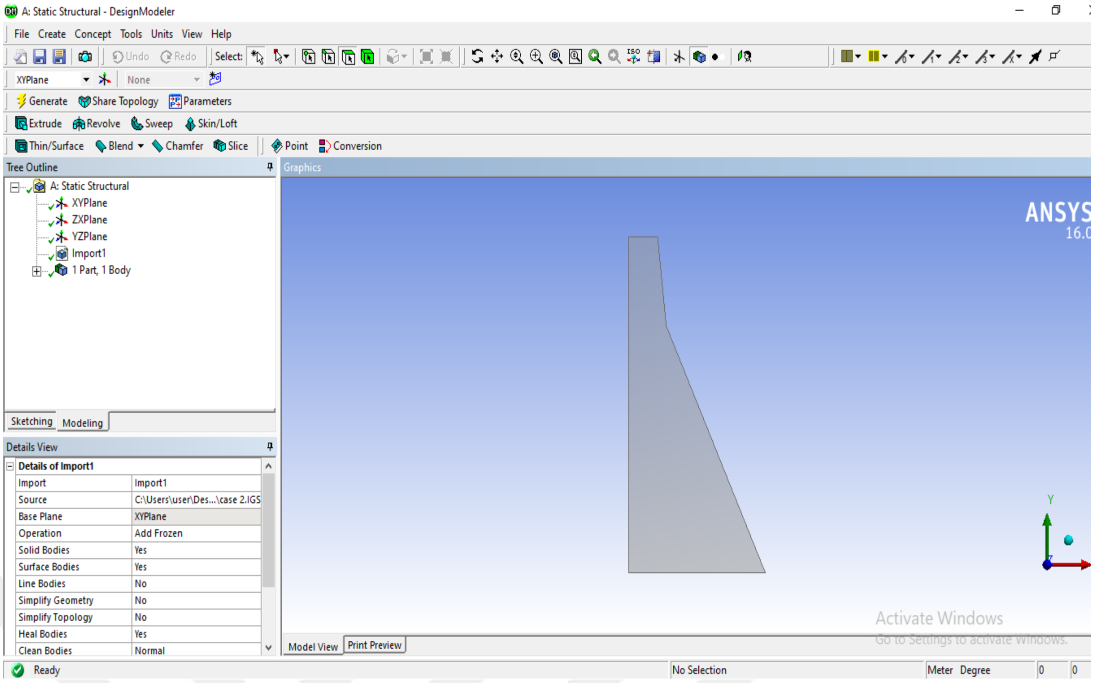

Figure 3.12 Import the dam geometry for second case of study

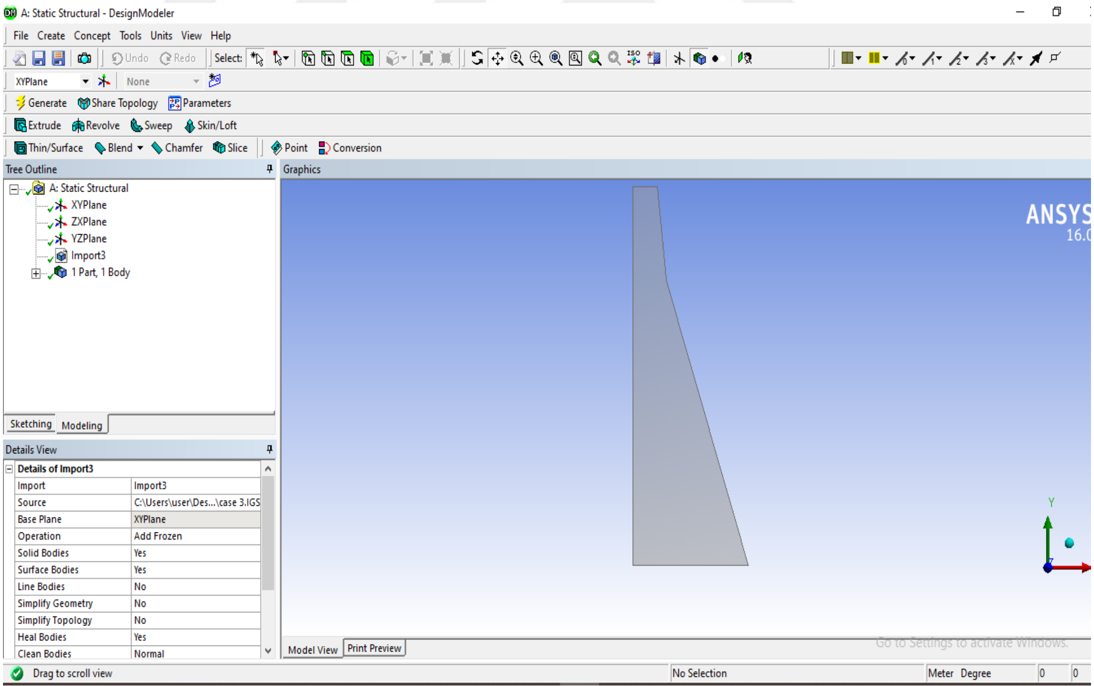

Figure 3.13 Import the dam geometry for third case of study

Understanding the model requires first developing a material model and then finding material attributes. These materials display the typical traits of those of average strength, and it is on these traits that the material's inherent features are founded. The Portland cement concrete was used extensively throughout the construction process.

4. Mesh formation

ANSYS allows users to access a wide variety of meshes. Several of the most often used mesh settings and meshing approaches can be accessed with a single click using the mesh tool (Menu>Preprocessor>Meshing>Mesh Tool). Afterwards, the geometry should mesh. The structural examination of the total volume of the dam requires the generation of a mesh. Creating a network of nodes and elements requires a formula that takes into account factors such as locality, element quality, and mesh controls. The Mesh Tool is a dynamic "toolbox" that can be used from the very beginning to the very end of the process. Even though all of the options it provides are available through regular ANSYS menus and commands, using the Mesh Tool is a time-saving shortcut (Figure 3.14).

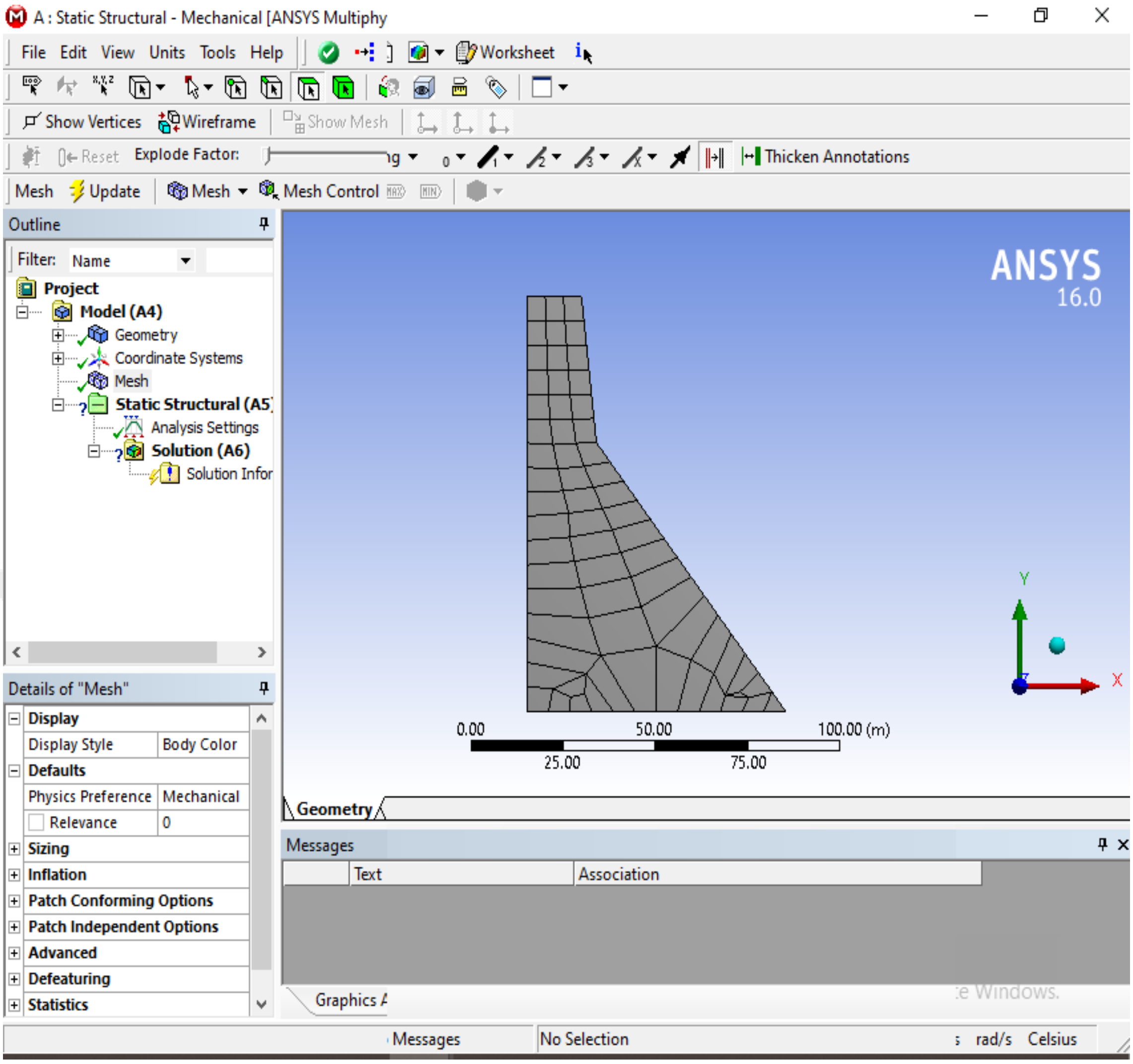

Figure 3.14 Meshing the dam geometry for third case of study

Using the size functions, all of the edges, faces, and volumes of a mesh can be scaled up or down. The case study must be discretized in light of the meshing outcomes. The shapes and sizes of the components of the 2-D mesh are quite adaptable. The mesh component generates a three-dimensional structure. You may customize the mesh's quality by determining the number and size of its constituent elements (Figure 3.15).

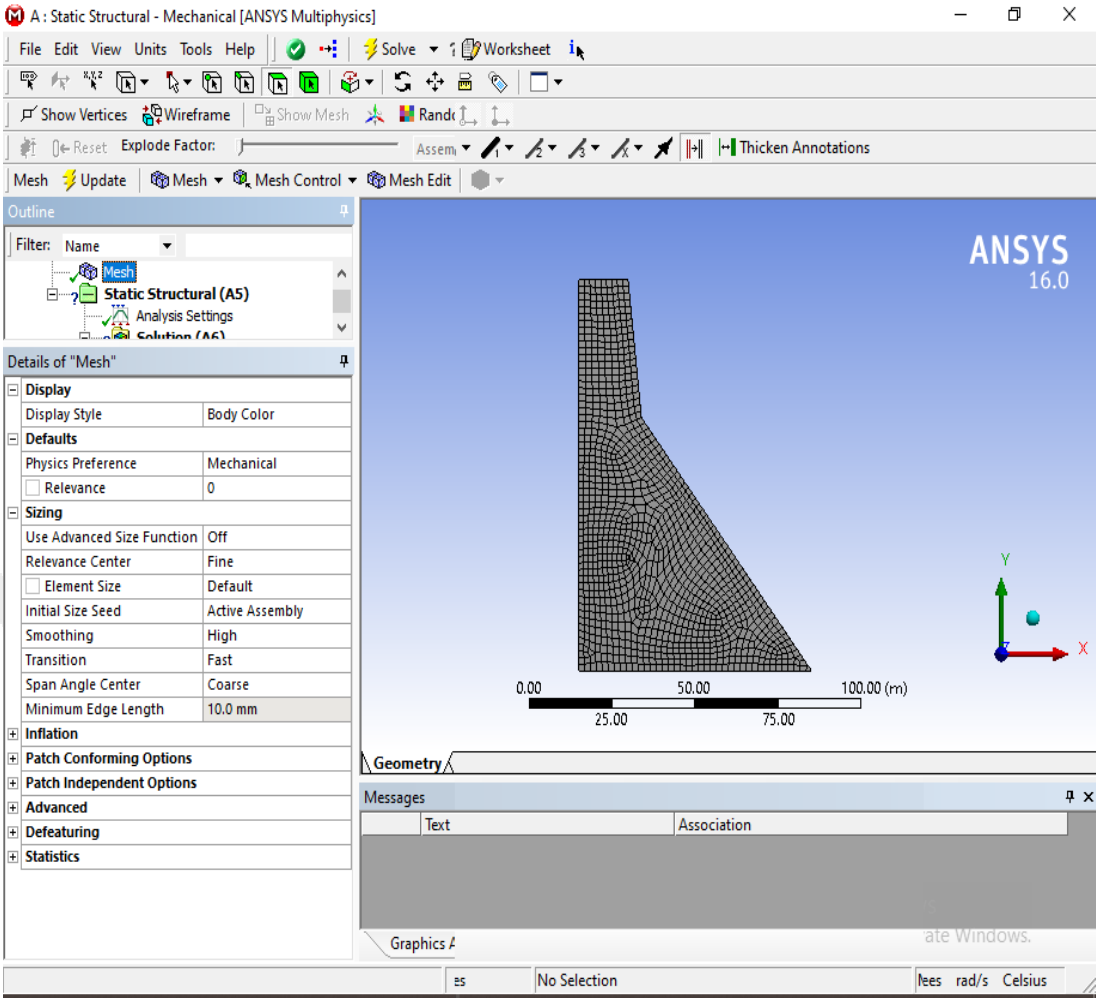

Figure 3.15 Refine the mesh

Problems with near-tangencies, topological design, etc., make mesh generation a challenging task. The term "mesh complexity" describes the process through which these intangibles are transformed into measurable quantities. Many geometries, for example, feature exceedingly complicated mathematical curves and surfaces that mesh in a very simple fashion. It is worth noting that the boundary layer can be discretized in a variety of ways, allowing for deeper analysis and more accurate results. Indicating the level of difficulty requires intricate meshing. I'm having trouble getting the geometry to mesh.

A model with a similar level of difficulty to mesh might be constructed by using linear curves and flat surfaces. As the researcher confirmed, the optimum mesh quality in ANSYS is between 0.5 and 0.8, which is in accordance with the skewness legislation (0.79).

5. Determine the loads

During the loading process, the ANSYS program can be used to determine accurate densities and other types of physical properties. The process of loading the model is an essential part of the simulation due to the fact that the quantity, nature, position, and trajectory of the load all play key roles in deciding how the model will react to the situation being simulated. The actual model used in this research demonstrated that the loading point of the structure is located somewhere in the middle of it. Examining how well the model works can be accomplished by first converting the data into Excel tables and then using those tables. On the form, detailed descriptions of each test are displayed next to the modification method and accompanying values. Also displayed are the results of each test. The load effectwill be computed once the forces have been distributed across the Mesh's elements and nodes in the body using a sequence of computations created from the infinite elements. When temperature is factored into the computations, it causes the model's response to change in accordance with the load that is being applied. Figure 3.16 indicates that this information should be considered part of the current phase. It has been established that static structural alternatives can provide inset possibilities depending on the conditions of both thermal load and static stress (Figure 3.17). In addition, the types of supports that can be used are restricted by the materials that are being used. The concrete that makes up the body of this artwork has been stressed in a number of different ways, as seen by the many different ways in which it appears (Figure 3.18).

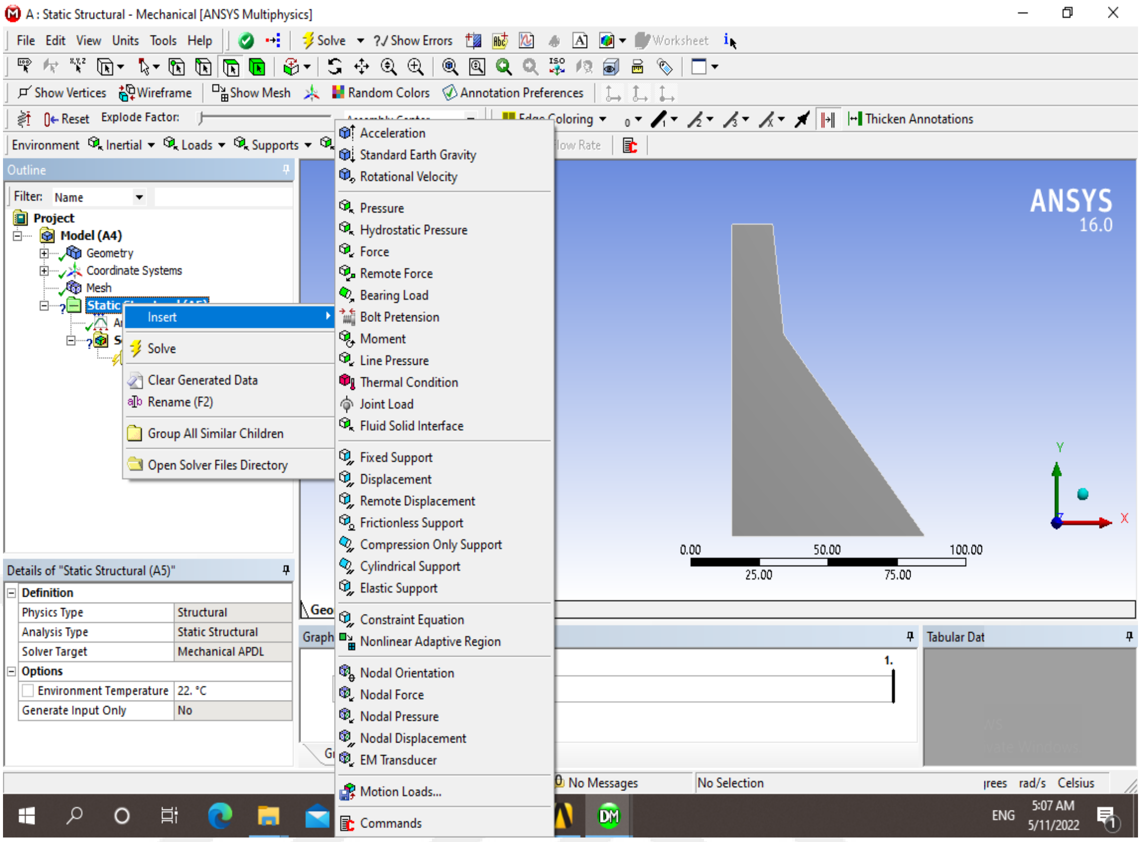

Figure 3.16 Loading on dam elements

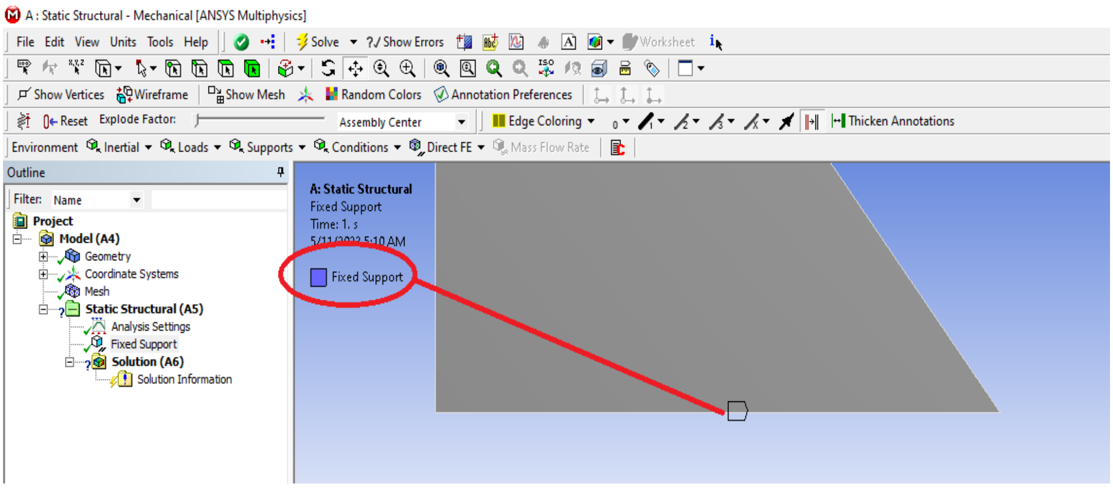

Figure 3.17 Fixed types and configuration of dam shape

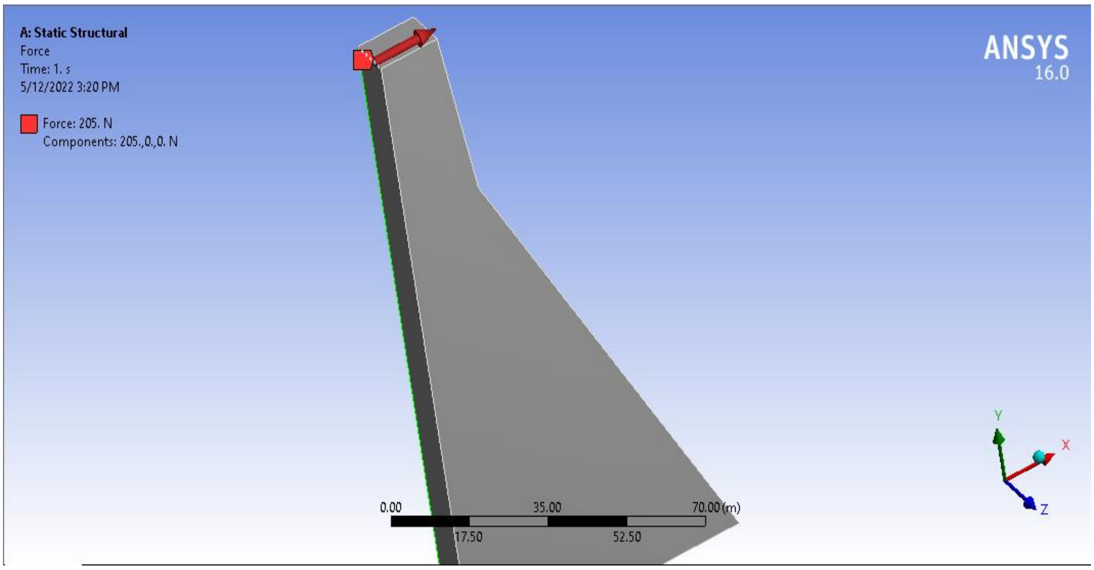

Figure 3.18 The same load condition applied in all cases

3.5 Solving Process

If the FE package's analysis component determines that the input file is error-free, the package will accept the file and run the necessary checks on the data it contains before continuing with the analysis and producing the output files. The input file will not be accepted if the FE package's analysis module cannot determine whether or not it contains errors. These should have a ton of data if the study was comprehensive. You can examine these files and pull useful information out of them, but there's usually so much data that it needs to be presented in a more approachable fashion. There is usually a lot of data available. It is the post-job processor's to see that this is taken care of. Most of the software packages used by pre-processors and post-processors are interchangeable. Information is presented to the user in tabular and graphical forms after being compiled by the post-processor from the output files. Using color to denote the value of a particular component's stress on the surface of the component, drawing contour lines of equal stress like in Figure 3.19 and Figure 3.20, or generating analogous displays on sections via the mode.

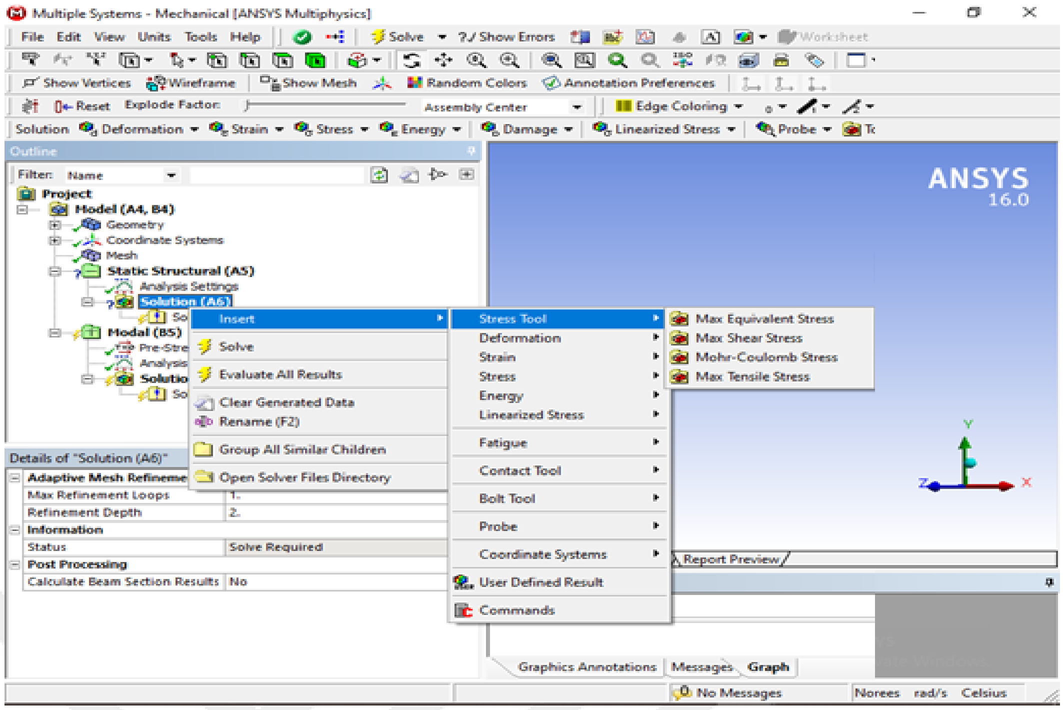

Figure 3.19 ANSYS solver using the deformity command

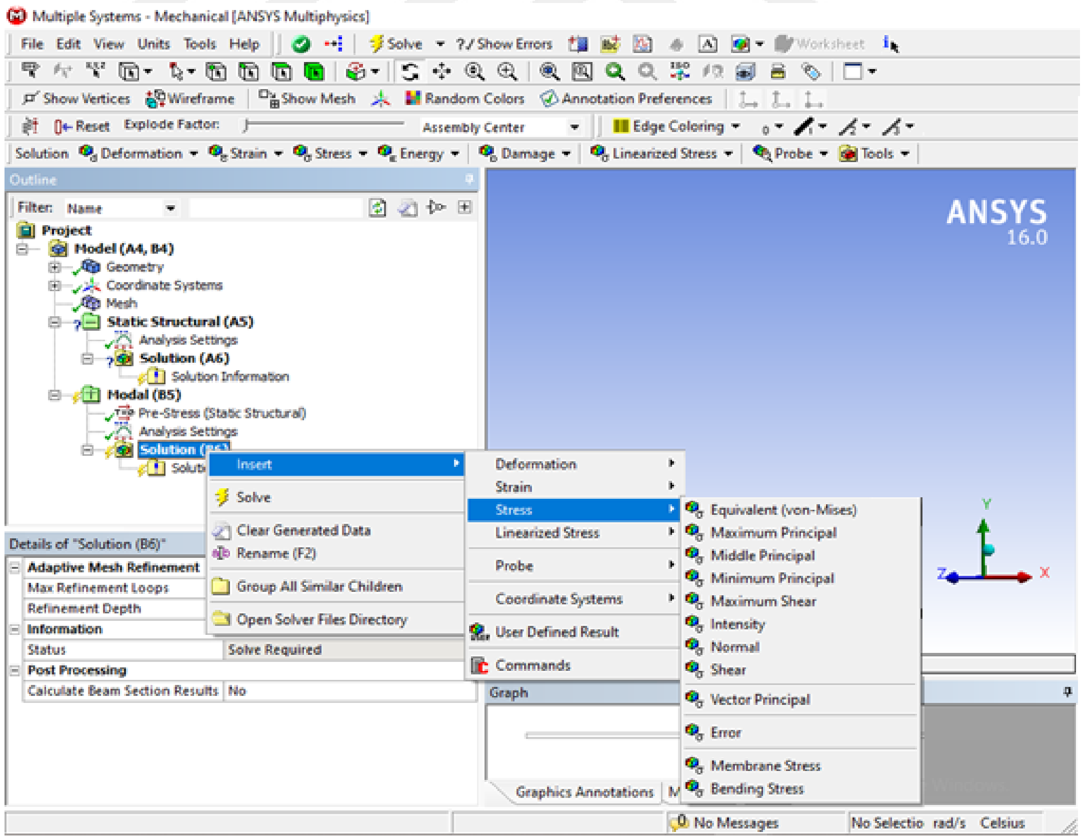

Figure 3.20 ANSYS solver using the stresses command

4. RESULTS AND DISCUSSION

Three types of dams were investigated experimentally, followed by numerical studies. This chapter also discusses how to create a numerical model and input material data to simulate nonlinear dam behavior, as well as comparing the behavior of conventional dams and those reinforced with high-density polyethylene fibers.

4.1 The Case Studies

Figure 4.1, Table 4.1, Table 4.2, and Table 4.3, depict the results of the tests conducted with two groups of conditions: conventional reinforced concrete and polypropylene fiber reinforced concrete. These tests were carried out in order to determine the relative strengths of the two types of concrete. Both traditional reinforced concrete and polypropylene fiber reinforced concrete were utilized throughout the course of the research. Both types of reinforced concrete were referred to as "conventional." The first group received a reinforcement of 12 millimeters, while the second group received the exact same dam shape but with polypropylene fiber reinforcement.

Table 4.1 The results of the trials

Dam Types	Crest Height	Dam Height	Width
Small crest	36.5	103	14.8
Medium crest	40	150	14.8
Long crest	50	200	14.8

The following is a summary of the experimental procedure: Since the volume percentage of HDPE fiber reinforcement is one of the most crucial factors, the researcher examined concrete under two separate conditions: conventional concrete and concrete with HDPE fiber reinforcement. In all other aspects, both circumstances were identical.

To determine the differences, the results of the laboratory tests will be utilized and then entered into the ANSYS simulation program. Total of the twenty-four distinct simulation exams that must be examined.

Table 4.2 Information about the trials

Test code	**Concrete conditions**	**No.of samples**
Wa 1-1	Traditional concrete	12
Wa 2-1	concrete with HDPE	12

Figure 4.1 Findings of the two types of concrete spacemen in order for all specimens tested

Table 4.3 Properties for reinforced and concrete compressive stress

HDPE size	**5 x 20 mm**
The 28 days compressive stress of concrete f'_c (MPa)	25
The 28 days compressive stress of concrete with polypropylene fiber reinforced f'_c (MPa)	26.45

4.2 Verification and Validation

The models described in this study are validated using experimental data, and a good model is chosen by configuring it with the right mesh approach and applying it to the right boundary condition. Verification and validation of the study are the topics of this subsection. The concrete dam is modeled using test parameters from an earlier investigation. This study shows how to create a reliable model and how to use it to describe certain behaviors.

4.2.1 Model validation

By comparing the results with a specially selected model from Koyna Dam, as stated by, the validation method ensures that the structural model is created in the right way and leads to a convincing illustration of reality (De Falco *et al.* 2017) (Figure 4.2).

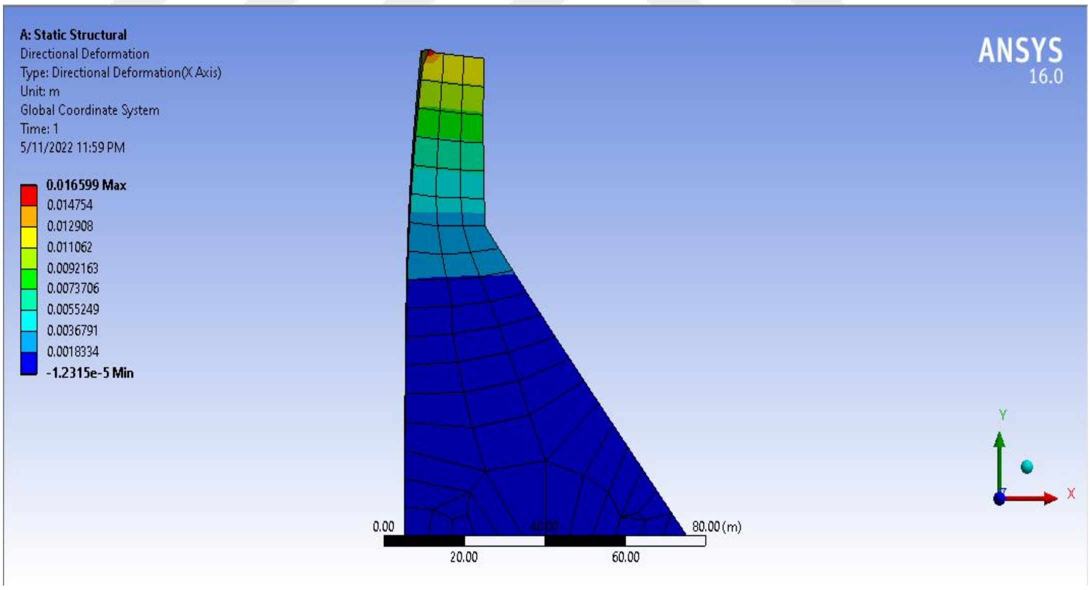

Figure 4.2 The result of the static structure

A confirmation model was developed, as stated in (De Falco *et al.* 2017), from experimental data gathered by applying various loads to the dam's crest in order to determine the displacement. In the investigation, the numerical findings are compared to the values that would be obtained if the experiment were conducted at ambient temperature (De Falco *et al.* 2017). The height of a dam is considered to be 103 meters, and its width is measured to be 14.8 meters, within the scope of this study. In both the analytical solution and the FE analysis, the applied load from overflow reflects a load that is generated by water flow and is applied to the crest of the dam (represent the head of dam). Altering the size of the model's overflow is one of the ways that the spectrum of dam deformation can be demonstrated. According to the findings of the FE analysis, which were in line with expectations, the displacement of a dam crest is proportional to the estimated deformation of the dam, and there is a clear relationship between the displacement and the subgrade modulus of the soil (Figure 4.3). In addition to this, the crest deformation will get worse as the overflow gets higher. Because the FE method is able to accurately predict the structural behavior of dams, it has become an important instrument in the field of engineering. The approach that has been suggested is applicable to every possible case involving dams that involves either unilateral contact loading or shared borders. An other choice is to do an analysis of the effects of the settlement of the dam (Table 4.4).

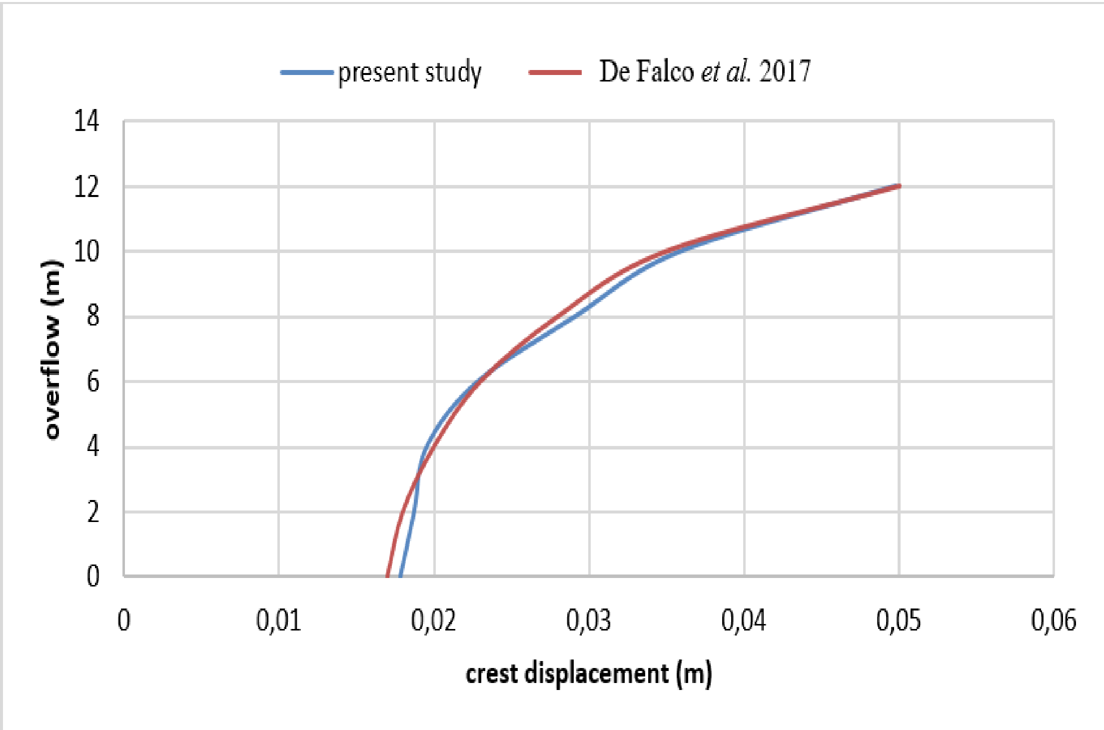

Figure 4.3 Comparison of De Falco *et al.* (2017) with the present study

Table 4.4 The numerical results comparison of present study and De Falco *et al.* (2017)

Water overflow (m)	(De Falco *et al.* 2017)	Present study	Error persentage
0	0.017	0.0178	4.71%
2	0.018	0.0187	3.89%
4	0.02	0.0195	2.50%
6	0.023	0.0228	0.87%
8	0.028	0.0291	3.93%
10	0.035	0.0359	2.57%
12	0.05	0.0498	0.40%

The following figures demonstrate how the curves derived from the FE analysis correspond to the laboratory test results obtained from the experiment. Although the FE analysis FE Model displacement curves are higher than the experimental displacement curves, the crest displacement curves of the FE analysis FE Model and the experimental displacement curves are very similar to one another. The end displacement of the FE analysis FE Model is found to be 0.0498 meters, which is smaller than the experimental ultimate overflow measurement of 0.05 meters. The peak displacement curves obtained from the FE analysis FE Model are consistent with the data obtained from the literature in earlier study (Table 4.4).

4.3 Results of Case 1

In order to model a dam, it is necessary to first translate the dimensions into a volume that represents the concrete body. Due to the symmetry in the geometry of both members, the FE analysis will employ a model that halves the dimensions of the steel supports and reinforcements. This section compares the typical overflow load to the displacement parameters of a concrete dam. The model considers gravity, the hydrostatic pressure that would exist if the reservoir were totally full, and the overflow pressure. During simulations of overflow, the model is self-weighted before the hydrostatic force is applied along the entire height of the dam. After that, the dam is subjected to a gradual, continuous increase in pressure due to overflow, beginning at the full reservoir water level and continuing until the dam hits the collapse limit condition. This pressure increase begins at the reservoir's full water level and continues until the dam reaches its limit of stability.

As depicted in Figure 4.4 and Figure 4.5, the behavior of the tested dam is constant over all load-displacement curves. These figures depict the differences between a standard concrete dam and an HDPE-reinforced concrete dam, as revealed by the FE Model study. In comparison to the experimental results, each of the FE numerical models forecasts a significant amount of final stage displacement.

Model displacements are measured in the X-direction at the FE model's crest face and denoted by the letter x. The load versus displacement curve is utilized so that the dam's findings may be compared to the experimental laboratory's data.

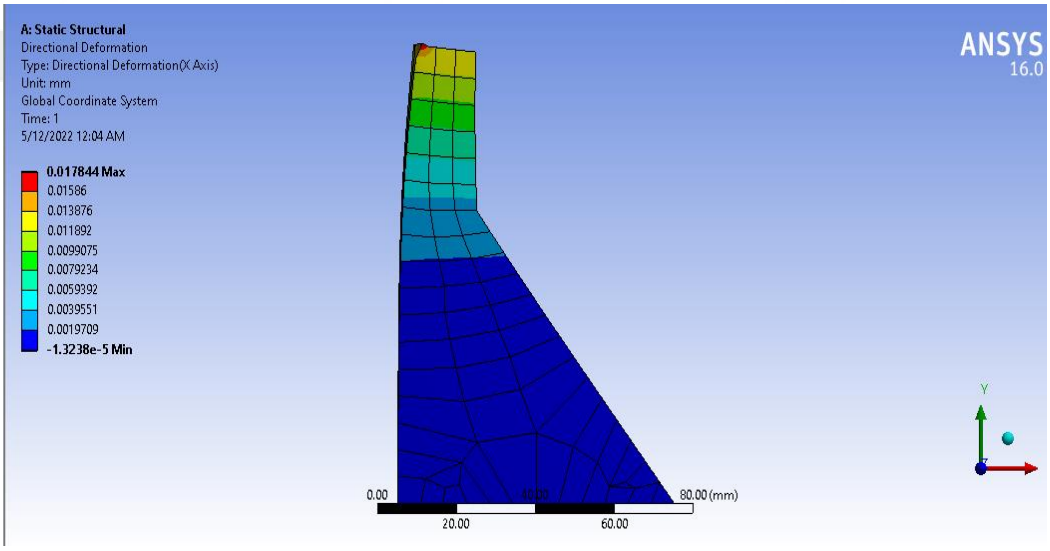

Figure 4.4 The crest displacement of HDPE concrete dam first case

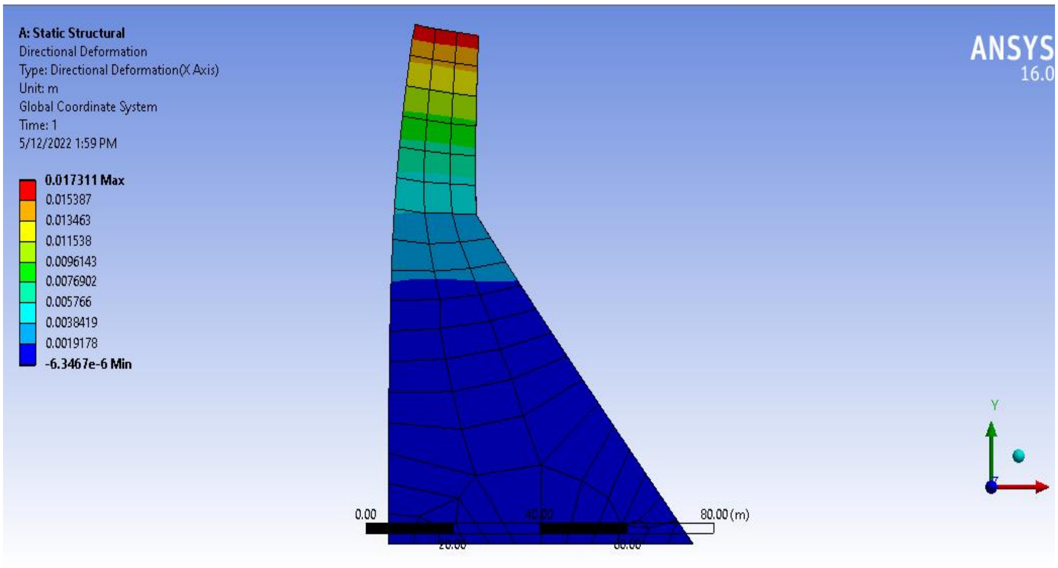

Figure 4.5 The crest displacement of concrete dam first case

Figure 4.6 shows how the curves from the FE analysis match the lab test results from the experiment. The experimental and FE analysis FE Model crest displacement curves match well, and the FE analysis; FE Model curves show a superior result of HDPE concrete than the typical concrete displacement curves. The FE analysis FE Model's end load for HDPE concrete is 0.049302 (m), but it was 0.051294 (m) based on the same overflow effect. Table 4.5 shows how the crest displacement curves from the FE analysis FE Model correlate nicely.

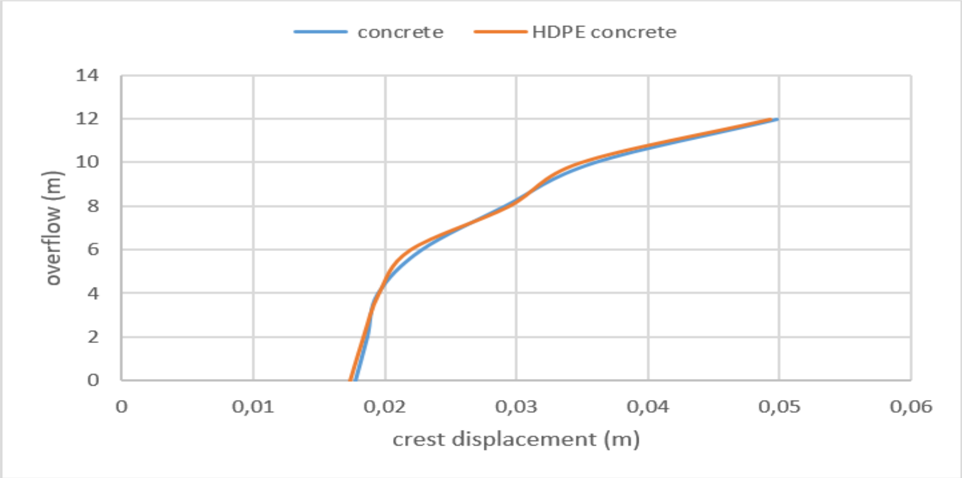

Figure 4.6 Comparison results of crest displacement between traditional concrete and HDPE concrete

Table 4.5 Numerical comparison results of crest displacement between traditional concrete and HDPE concrete

Water overflow (m)	Concrete	Hdpe concrete
0	0.0178	0.017311
2	0.0187	0.018326
4	0.0195	0.0195
6	0.0228	0.021888
8	0.0291	0.029391
10	0.0359	0.034823
12	0.0498	0.049302

4.4 Results of Case 2

The technique for modeling continues with the construction of a new volume of dam model, which entails modifying the proportions of the concrete body in order to achieve the desired results. Because of the symmetry that exists in the geometry of both members, the steel supports and reinforcements will be treated as being half their actual size for the FE analysis. In order to accommodate for this, extra boundary restrictions that run perpendicular to the axis of symmetry must be implemented. All displacement curves for the tested dam have been compared, with all FE numerical models displaying significant displacement at the final stage, as shown in Figure 4.9. The differences in FE Model analysis between a typical concrete dam and an HDPE-reinforced concrete dam are depicted in Figure 4.7 and Figure 4.8, respectively.

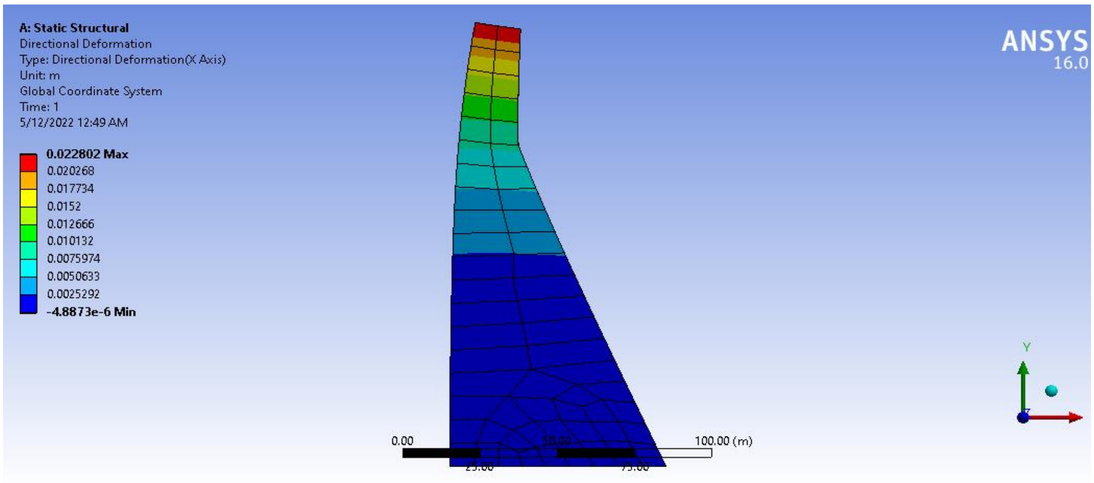

Figure 4.7 The crest displacement of HDPE concrete dam second case

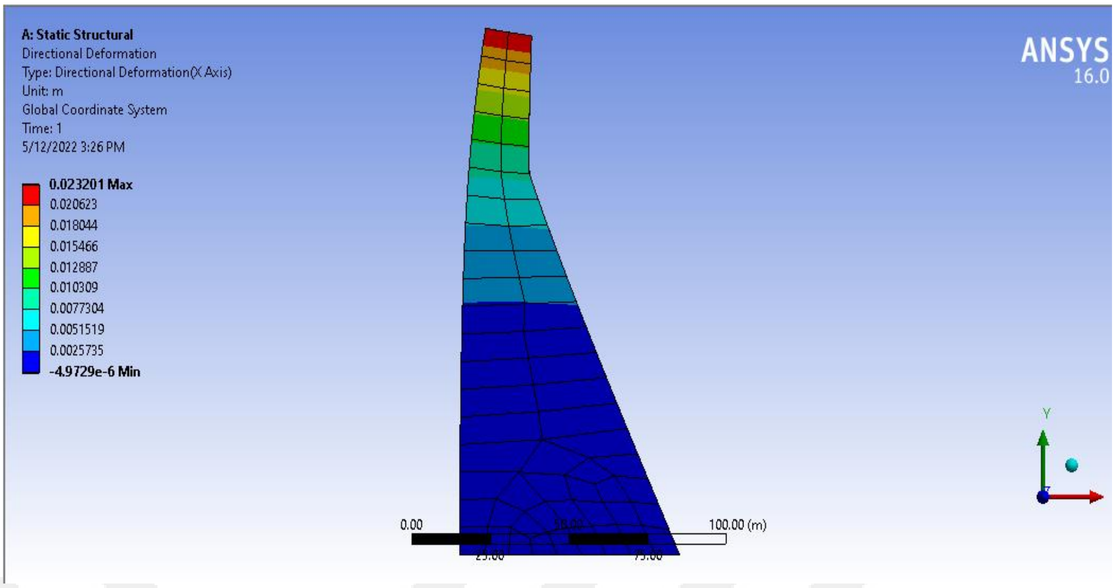

Figure 4.8 The crest displacement of concrete dam second case

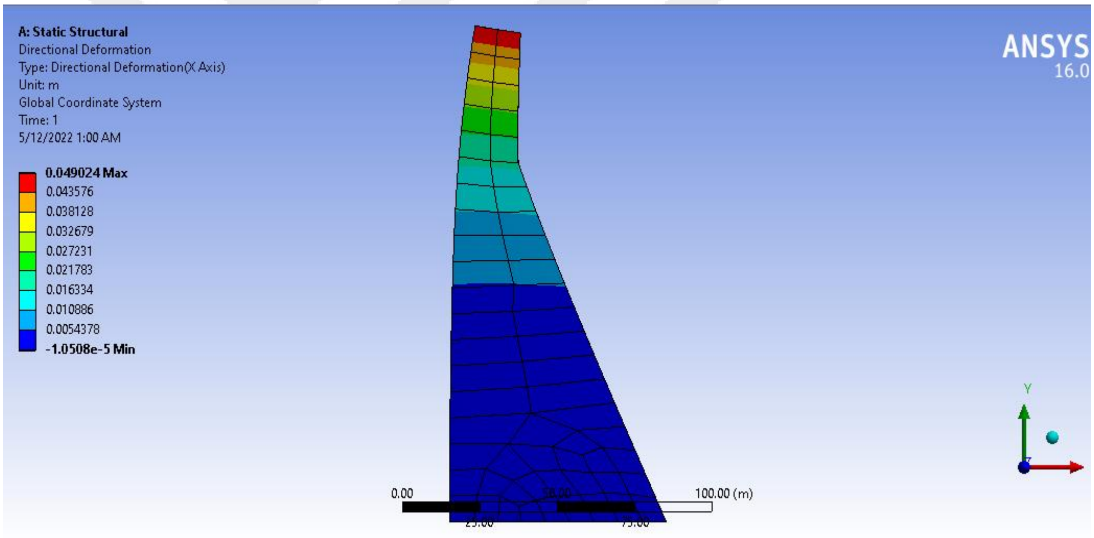

Figure 4.9 The highest overflow of crest displacement of HDPE concrete dam second case.

During simulations of overflow, the model is self-weighted before the hydrostatic force is applied along the entire height of the dam. After that, the dam is subjected to a gradual, continuous increase in pressure due to overflow, beginning at the full reservoir water level and continuing until the dam hits the collapse limit condition. This pressure increase begins at the reservoir's full water level and continues until the dam reaches its limit of stability. As previously discussed, the X-direction showing of Ux is utilized to identify the model's movement in that direction. The ratio of mass to volume. Figure 4.10 depicts the curves that were created by the FE investigation. The crest displacement curves for both scenarios are extremely similar, and the FE Model displacement curves reveal that HDPE concrete performs substantially better than ordinary concrete. Due to the same overflow effect, the final load predicted by the FE analysis FE Model for HDPE concrete was 0.0490 meters, whereas the actual value was 0.0644 meters. The correlation between the crest displacement curves from the FE analysis and the FE Model is depicted in Table 4.6.

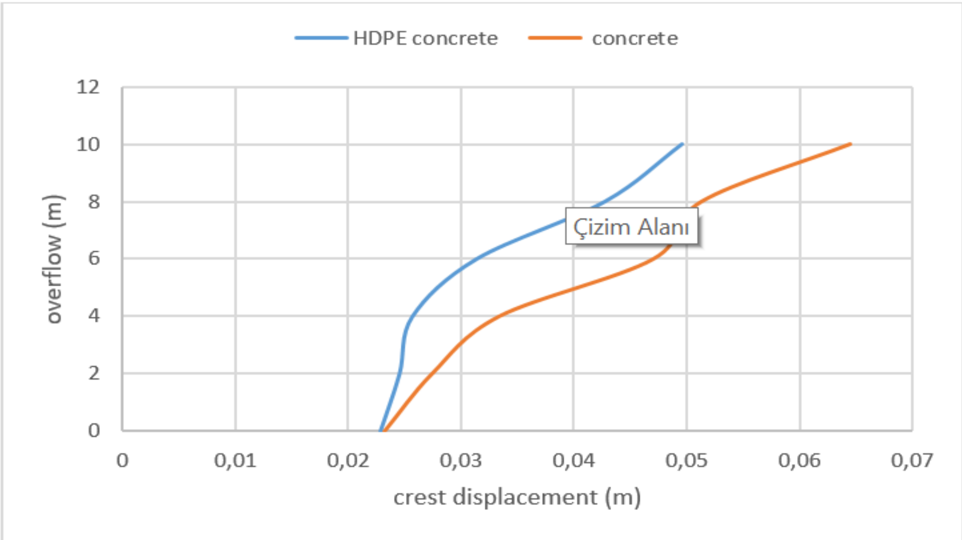

Figure 4.10 Comparison results of crest displacement between traditional concrete and HDPE concrete of second case

Table 4.6 Numerical comparison results of crest displacement between traditional concrete and HDPE concrete of second case

Water overflow (m)	Hdpe concrete	Concrete
0	0.0228	0.023201
2	0.0245	0.0274
4	0.02565	0.033345
6	0.03135	0.047025
8	0.04275	0.0513
10	0.0490	0.06448

4.5 Results of Case 3

In the concluding phase of the modeling technique, you will create a highrise volume of dam dimensions for the long crest concrete body. This will be accomplished utilizing the dimensions of the dam. Due to this, extra boundary constraints that are perpendicular to the symmetry axis must be implemented. In this specific example, the height of the dam is 200 meters. It compares the estimated load from the water overflow to the displacement characteristics of the concrete dam. Real-world circumstances can be observed in the model, demonstrating that both are susceptible to overflow. As shown in Figure 4.11 and Figure 4.12, the overflow generated a displacement, which finally resulted in a step-by-step constant pressure effect. In the analysis conducted using the FE Model, there are differences between a conventional concrete dam and an HDPE-reinforced concrete dam, and all displacement curves under the investigated conditions are shown in Figure 4.13.

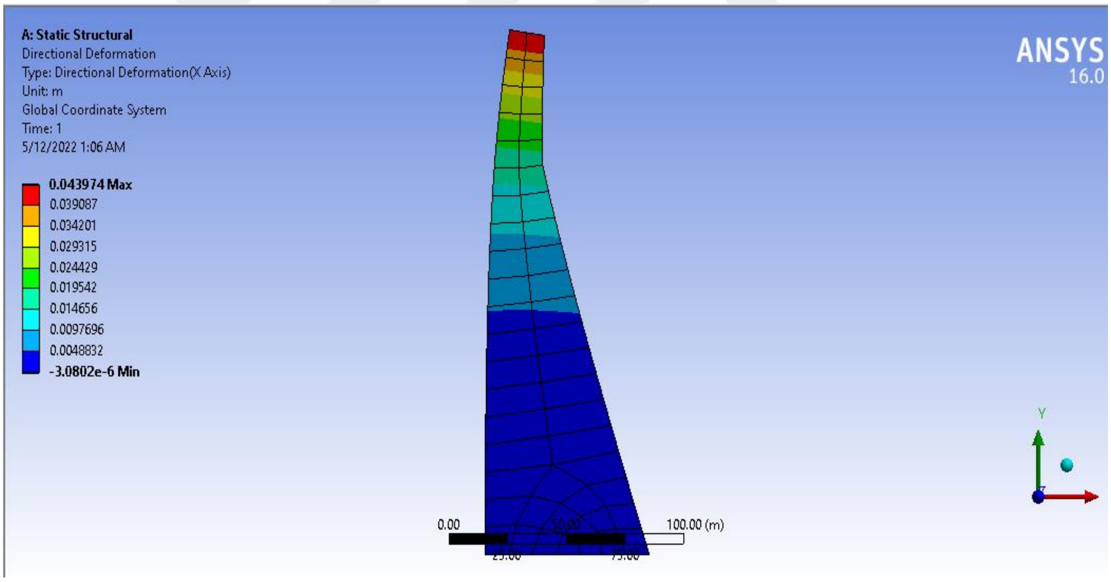

Figure 4.11 The crest displacement of HDPE concrete dam third case

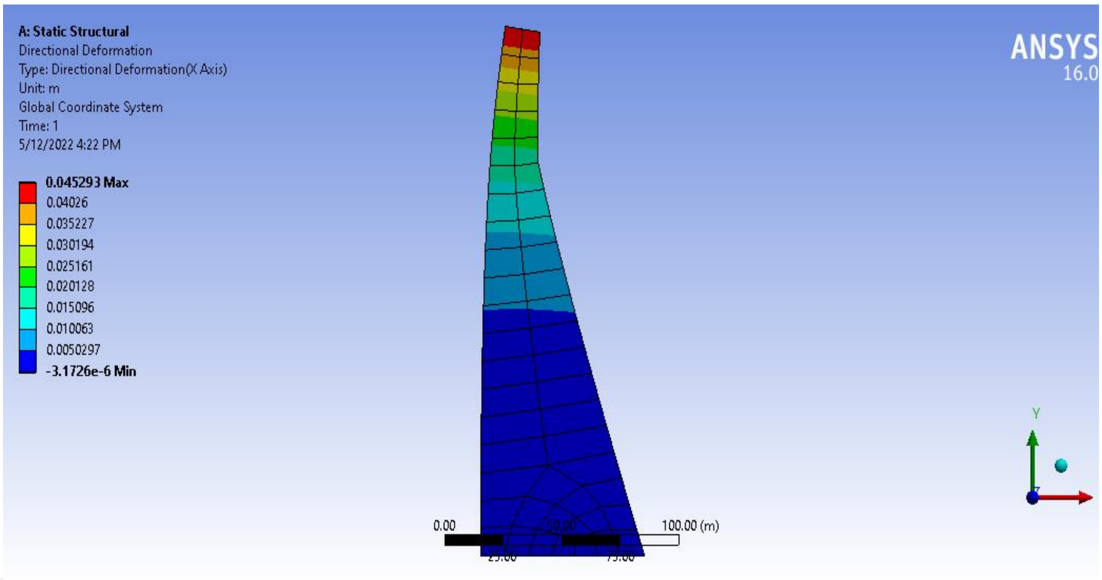

Figure 4.12 The crest displacement of conventional concrete dam third case

Figure 4.13 shows the curves from the FE study. HDPE concrete produced a superior crest displacement result than typical concrete displacement curves. Table 4.7 shows how the crest displacement curves from the FE analysis FE Model match up nicely.

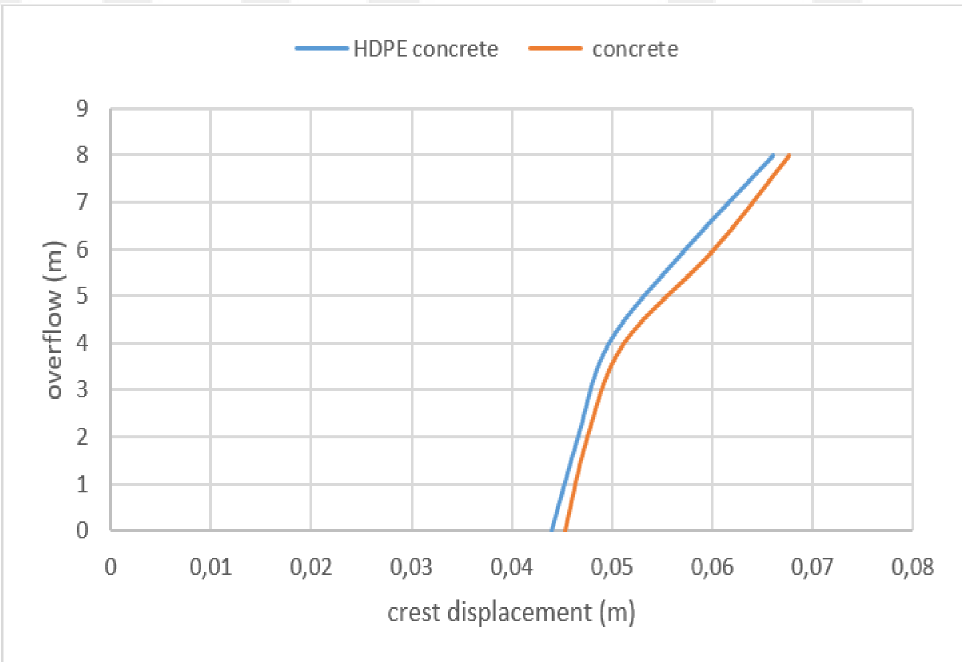

Figure 4.13 Comparison results of crest displacement between traditional concrete and HDPE concrete

Table 4.7 Numerical comparison results of crest displacement between traditional concrete and HDPE concrete

Water overflow (m)	Hdpe concrete	Concrete
0	0.04397	0.045293
2	0.0466	0.047532
4	0.0497	0.051191
6	0.05736	0.060228
8	0.06512	0.0677248

Due to this weight, the uppermost concrete layers will be compacted, resulting in a reduced length, while the ones below will be elongated (stretched). As the weight continues to be applied, the beam begins to droop and cracks emerge on the lower half of the face, resulting in the beam's eventual failure. This is due to the relatively low tensile strength of concrete. Cracking occurs when structural concrete is subjected to mechanical stress, which has an adverse influence on the transport qualities of the concrete, but this effect is not well understood. The analysis demonstrates a large variance in experimentally generated permeability statistics, which appears to be mostly attributable to the use of distinct test procedures. This difference was revealed as a result of the investigation. It is unclear whether equilibrium was reached in the fluid flow, nor whether flow measurements were taken while tension was being applied; hence, it is not possible to compare the results of the several trials. Nevertheless, it is evident that stress-induced cracking increases fluid flow, and there is a threshold value for both the applied stress and the resulting fracture width in concrete, which is proportional to the permeability of the fluid. Both of these variables are related to the fluid's permeability. Figure 4.14 depicts the position of the greatest tension in this type of concrete.

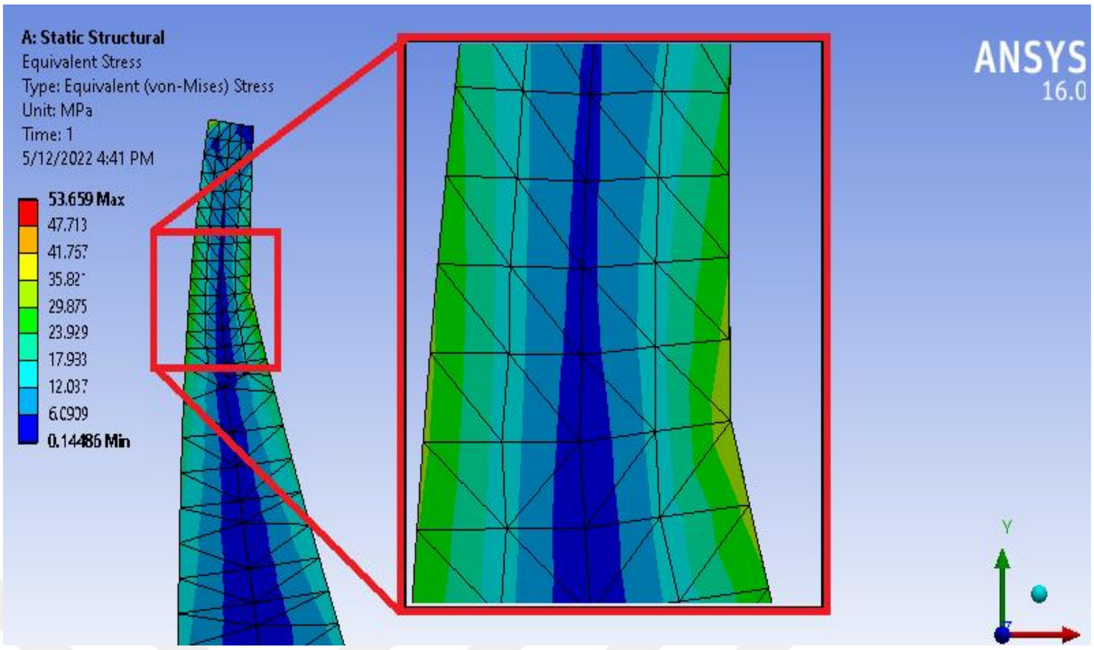

Figure 4.14 The maximum stress position

5. CONCLUSIONS AND RECOMMENDATION

In comparison to other results discovered in the literature, the numerical results of the overflow analysis demonstrate that the first model can replicate the behavior of other plasticity models and that the given models can capture the load displacement behavior of fracture mechanics models. In addition, the first model can mimic the behavior of other fracture mechanics models. According to the results of the transient experiment, both models can accurately forecast the shear load and displacement histories of the Koyna Dam in the presence of the overflow effect. The first provides just a rough crack initiation point, but it is able to record the history of the force produced by the failure and its size. The prediction of fracture propagation is essentially erroneous due to the limited ways in which cracks can spread. The second one is more promising since it depicts the entire amount of damage and the structural response to displacements more accurately. It has numerous advantages, especially from a pragmatic standpoint. The improvement in convergence of the FE analysis can be partially attributable to the availability of the explicit form of the constitutive law and the tangent matrix. In contrast, the capacity to actively manage different types of fracture stresses enables researchers to see distinct failure patterns (sliding-rocking). There is no need to revisit previously failing regions and fix them. In this chapter, we discuss the achievements of the research process as well as the efforts taken to fill research gaps. The most essential contribution of this work is an investigation of the fundamental differences between a concrete dam and one made of HDPE-reinforced plastic. The objective of this thesis is to analyze the movement of a dam's crest under varied loads and in the presence of a range of subgrade modulus effects and to conclude how this movement occurs. The following issues can be deduced from the work completed to date:

- The displacement response and overflow behavior in concrete dams agree surprisingly well, according to the results of FE analytical experiments conducted on three separate scenarios.
- The optimal improvement was achieved when HDPE fiber was added to dam concrete with a high load impact. This resulted in the greatest enhancement.

5.1 Future Works

In the future, it will be required to perform a new examination for concrete materials, such as higher-grade mixtures, in order to expose the two different kinds of concrete that have been used on other dams due to the different circumstances.

REFERENCES

Achilleos, C., Hadjimitsis, D., Neocleous, K., Pilakoutas, K., Neophytou, P. O. and Kallis, S. 2011. Proportioning of steel fibre reinforced concrete mixes for pavement construction and their impact on environment and cost. Sustainability, 3(7): 965-983.

ACI Committee. 2014. Building code requirements for structural concrete (ACI 318-14) and commentary. American Concrete Institute, 465 page, New York.

Aire, C., Mendoza, C. and Davila, P. 2011. Polypropylene fibers reinforced concrete: optimization on plastic shrinkage cracking. In Proceedings of the Second International Conference on Future Concrete. Abu Dhabi, UAE, 12.

Appiah, J. K., Berko-Boateng, V. N. and Tagbor, T. A. 2017. Use of waste plastic materials for road construction in Ghana. Case Studies in Construction Materials, 6: 1-7.

Ariyan, M., Habibagahi, G. and Nikooee, E. 2016. Seismic response of earth dams considering dynamic properties of unsaturated zone. In E3S Web of Conferences, EDP Sciences, 16(9).

Arna'ot, F. H., Abbass, A. A., Abualtemen, A. A., Abid, S. R. and Özakça, M. 2017. Residual strength of high strength concentric column-SFRC flat plate exposed to high temperatures. Construction and Building Materials, 154: 204-218.

Behfarnia, K. and Sayah, A. R. 2012. FRP strengthening of shear walls with openings. Asian Journal of Civil Engineering, 13(5): 691-704.

Berton, R., Mazloumi, A. and Ghaemian, M. 2009. Estimation of fracture parameters using experimental test results for non-linear seismic analysis of Jahgin RCC gravity dam. Dam Engineering, 20(1): 5.

Campos, A., López Garello, C. M., Blanco Álvarez, A. and Aguado de Cea, A. 2016. Structural diagnosis of a concrete dam with cracking and high non-recoverable displacements. Journal of Performance of Constructed Facilities, 30(5): 04016021-1.

Chi, Y., Xu, L. and Zhang, Y. 2014. Experimental study on hybrid fiber–reinforced concrete subjected to uniaxial compression. Journal of Materials in Civil Engineering, 26(2): 211-218.

Chowdhury, M. A. and Hossain, S. 2020. A review on tensile and flexural properties of Fiber-reinforced polymer composites. Journal of Polymer Science Part A: Polymer Chemistry, 7: 16-26.

De Falco, A., Mori, M., Sevieri, G. and Zani, N. 2017. Simulation of concrete crack development in seismic assessment of existing gravity dams. Torrossa Online Digital Bookstore, 92-102.

Deoda, V., Adhikary, S. and Srinivasa, R. V. 2020. Seismic analysis of earthen dams subjected to spectrum compatible and conditional mean spectrum time histories. Jordan Journal of Civil Engineering, 14(1).

Engel, T., Lechler, A. and Verl, A. 2014. Adaptive friction bearing for reduction of stick-slip effects. In Advanced Materials Research, 1018:351-356.

Getachew, H. 2018. Evaluation of dynamıc stability of embankment dam. MSc. Thesis, Addis Ababa University, 77 page, Addis Ababa.

Godfrey, L. 2019. Waste plastic, the challenge facing developing countries—ban it, change it, collect it?. Recycling, 4(1): 3.

Hasan, M. J., Afroz, M. and Mahmud, H. M. I. 2011. An experimental investigation on mechanical behavior of macro synthetic fiber reinforced concrete. International Journal of Civil & Environmental Engineering, 11(3): 19-23.

Ismail, Z. Z. and Al-Hashmi, E. A. 2008. Use of waste plastic in concrete mixture as aggregate replacement. Waste Management, 28(11): 2041-2047.

Jagota, V., Sethi, A. P. S. and Kumar, K. 2013. Finite element method: An overview. Walailak Journal of Science and Technology, 10(1): 1-8.

Jaiswal, O. R. and Jain, S. K. 2004. Simple tuned mass damper to control seismic response of elevated tanks. In Proceedings of the 13th World Conference on Earthquake Engineering, 2004(8): 1-6.

Khayoun, Z. I., Kamal, H. M. and Ibrahim, Y. K. 2020. The effect of hybrid fibers reinforcement on the mechanical and physical properties of concrete. The Open Civil Engineering Journal, 14(1).

Lasiyal, N., Pawar, G. S. and Dixit, M. 2016. Effect of plastic waste as partial replacement of fine aggregate in concrete and cost analysis. International Journal of Engineering Reseach and Technology, 4(23): 1-4.

Li, Z., Wu, M., Wu, J., Cui, Y. and Xue, X. 2020. Steel fibre reinforced concrete meso-scale numerical analysis. Advances in Civil Engineering, 2020(1).

Liang, H., Guo, S., Tian, Y., Tu, J., Li, D. and Yan, C. 2020. Probabilistic seismic analysis of the deep sliding stability of a concrete gravity dam-foundation system. Advances in Civil Engineering, 2020(1).

Löfgren, I. 2005. Fibre-reinforced concrete for industrial construction. PhD. Thesis, Chalmers University of Technology, 277 page, Göteborg.

Meran, C., Ozturk, O. and Yuksel, M. 2008. Examination of the possibility of recycling and utilizing recycled polyethylene and polypropylene. Materials & Design, 29(3): 701-705.

Mohammadi, S. 2008. Extended finite element method: for fracture analysis of structures. John Wiley & Sons, 280 page, New York.

Mohod, M. V. 2015. Performance of polypropylene fibre reinforced concrete. IOSR Journal of Mechanical and Civil Engineering, 12(1): 28-36.

Nikbin, I. M., Rahimi, S., Allahyari, H. and Fallah, F. 2016. Feasibility study of waste Poly Ethylene Terephthalate (PET) particles as aggregate replacement for acid erosion of sustainable structural normal and lightweight concrete. Journal of Cleaner Production, 126: 108-117.

Nurdiana, J. 2021. The effect of recycled HDPE plastic additions on concrete performance. Recycling, 6(1): 18.

Panfilov, I. A., Soloviev, A. N., Matrosov, A. A., Meskhi, B. C., Polushkin, O. O., Rudoy, D. V. and Pakhomov, V. I. 2020. Finite element simulation of airflow in a field cleaner. In IOP Conference Series: Materials Science and Engineering. IOP Publishing, 1001(1): 12-60.

Pashazadeh, A. and Chekani-Azar, M. 2011. Estimating an appropriate plastic concrete mixing design for cutoff walls to control leakage under the earth dam. Journal of Basic and Applied Scientific Research, 1(9): 1295-1299.

Pelecanos, L. 2013. Seismic response and analysis of earth dams. PhD. Thesis, Imperial College London, 409 page London

Rahman, T. and Nurdiana, J. 2020. The effect of HDPE plastic fibres on concrete performance. Preprints, 21(6): 1-8.

Ravishankar, K. and Jeevanantham, K. 2021. Experimental investigatıon on high strength concrete with polypropylene fiber. International Research Journal of Engineering and Technology, 21(8): 1-7.

Seiphoori, A., Haeri, S. M. and Karimi, M. 2011. Three-dimensional nonlinear seismic analysis of concrete faced rockfill dams subjected to scattered P, SV, and SH waves considering the dam–foundation interaction effects. Soil Dynamics and Earthquake Engineering, 31(5-6): 792-804.

Shi, Z., Wu, Z., Gu, C., Chen, B., Zhang, H., Yin, W. and Wu, B. 2019. Calculation methods for the permeability coefficient of concrete face rockfill dam with cracks. Advances in Civil Engineering, 2019.

Silva, A. L. P., Prata, J. C., Walker, T. R., Campos, D., Duarte, A. C., Soares, A. M. and Rocha-Santos, T. 2020. Rethinking and optimising plastic waste management under COVID-19 pandemic: policy solutions based on redesign and reduction of single-use plastics and personal protective equipment. Science of the Total Environment, 742: 140565.

Silveira, I. V. and Pedroso, L. J. 2018. Analysis of natural frequencies and modes of vibration involving interaction dam-reservoir-foundation for concrete gravity dams. In Third International Dam World Conference, 18(11).

Varadarajan, A., Sharma, K. G., Abbas, S. M. and Dhawan, A. K. 2006. Constitutive model for rockfill materials and determination of material constants. International Journal of Geomechanics, 6(4): 226-237.

Wieland, M. and Fan, B. H. 2004. The activities of the international commission on large dams (ICOLD) in the earthquake safety of large dams. In Proceedings of the 13th World Conference on Earthquake Engineering, 4(8): 1-7.

Won, M. S. and Kim, Y. S. 2008. A case study on the post-construction deformation of concrete face rockfill dams. Canadian Geotechnical Journal, 45(6): 845-852.

Wu, B., Wu, Z., Chen, B., Su, H., Bao, T. and Wang, S. 2016. Crack status analysis for concrete dams based on measured entropy. Science China Technological Sciences, 59(5): 777-782.

Xu, L., Li, B., Ding, X., Chi, Y., Li, C., Huang, B. and Shi, Y. 2018. Experimental investigation on damage behavior of polypropylene fiber reinforced concrete under compression. International Journal of Concrete Structures and Materials, 12(1): 1-20.

Yadav, A. K., Prasad, B., Kumar, V. and Mohan, M. 2017. Properties of polypropylene fiber reinforced concrete and structural behaviour of beam. International Journal Innovative Research Science Engineering Technology, 6(6): 10200–10210.

Yimer, M. A. and Aure, T. W. 2020. Seismic performance of steel fiber reinforced concrete Beam-column joints under the variation of column axial load. Iranian Journal of Science and Technology, Transactions of Civil Engineering 46(3): 2249-2273.

Zienkiewicz, O. C., Taylor, R. L. and Zhu, J. Z. 2005. The finite element method: its basis and fundamentals. Elsevier, 752 page, Amsterdam.